Upper Cretaceous Tethyan Phosphogenic Province in the Qena-Idfu District, Egypt: Insights from Geology, Petrography, and Geochemistry

Fatma S. Ramadan , Abdel-Aal M. Abdel-Karim , Mokhles K. Azer , Hossam K. Sharaka * , Ahmed M. Khalil

Posted Date: 2 March 2026

doi: 10.20944/preprints202603.0009.v1

Keywords: Duwi Formation; Egypt; phosphorites; rare earth elements (REEs); Upper Cretaceous; uranium

 doi:10.20944/preprints202603.0009.v1

Article

Upper Cretaceous Tethyan Phosphogenic Province in the Qena-Idfu District, Egypt: Insights from Geology, Petrography, and Geochemistry

Fatma S. Ramadan [1], Abdel-Aal M. Abdel-Karim [1], Mokhles K. Azer [2], Hossam K. Sharaka [3,*] and Ahmed M. Khalil [3]

[1] Geology Department, Faculty of Science, Zagazig University, 44519 Zagazig, Egypt
[2] Geological Sciences Department, National Research Centre, 12622 Cairo, Egypt
[3] Mineral Resources & Mining Industries Authority, 11517 Cairo, Egypt
* Correspondence: hossam.sharaka_2014@yahoo.com; Tel.: +020-1093586814

Abstract

The Upper Campanian phosphorite series in Egypt, which overlies the Nubian Group, exhibits pronounced lateral lithological variations. Glauconitic, dolomitic, calcareous, and cherty sediments, together with bituminous shales, form diverse lithofacies associations that reflect the region's complex depositional environments. These lithofacies, associated with the Duwi Formation, are marine deposits originally formed in anoxic, organic-rich environments and later reworked into shallower, oxygenated settings during sea-level fluctuations. This study presents a detailed geological, petrographic, and geochemical characterization of these phosphorite deposits in North Aswan, Egypt, across five localities: Wadi Hilal, East Sibaiya, Um Higarah, Um Salama, and Um Tundbah. The lithostratigraphic succession is dominated by the Upper Cretaceous Duwi Formation, which unconformably overlies the Middle-Campanian Qusseir shale and conformably underlies the Middle-Maastrichtian Dakhla shale. Petrographically, the phosphorites comprise phosphatic grains (pellets and bioclasts such as bone fragments and shark teeth), non-phosphatic grains (quartz), and cements of silica, calcite, and iron oxides. Geochemically, P_2O_5 content ranges from 17.4 to 31.24%, uranium concentrations vary between 40.59 and 245.84 ppm, and total rare earth elements (∑REEs) range from 47.83 to 270.37 ppm. The studied phosphorites are suitable for phosphoric acid production, with potential for uranium recovery as a by-product.

Keywords: Duwi Formation; Egypt; phosphorites; rare earth elements (REEs); Upper Cretaceous; uranium

1. Introduction

Phosphorites are economically significant sedimentary deposits formed through the marine accumulation of organic matter and biogenic apatite. In Egypt, Upper Cretaceous (Campanian–Maastrichtian) phosphatic units of the Duwi Formation constitute one of the region's most important mineral resources. Phosphate reserves in Egypt are substantial, exceeding three billion metric tons [1,2]. The sedimentary sequence of the study area attracted the attention of many authors, among them [3–16].

The phosphate-bearing succession was first considered as a formation by [17] in the Qusseir district, who called it the "Phosphate Formation". Ref. [18] Gave this unit the widely accepted formal name, the "Duwi Formation", the typical locality Gebel Duwi, Qusseir area along the Red Sea coast. It overlies the variegated shales. In Egypt, this belt spans the Red Sea, Nile Valley, and Western Desert, forming widespread shallow-marine phosphatic facies associated with carbonates, organic-rich shales, chert, and glauconitic sandstones [19].

 doi:10.20944/preprints202603.0009.v1

Ref. [1] subdivided the Egyptian phosphatic into three trending facies belts: the phosphorite of the northern facies belt, spread from Bahariya Oasis to Sinai, that related to no economic potential that occur as thin layers of carbonate and sand facies; the central facies belts, that confined to the Safaga-Qusseir & Qena-Idfu & Kharga and Dakhla Oasis of economic occurrences; the southern facies belt lies south of latitude 22° N, these facies are associated with iron ore accumulation among shallow water sediments. The rare earth elements (REEs) were first tackled by [20], who reported the REEs abnormality in Abu Tartur phosphorites. Ref [21] Noted that the phosphorites of Abu Tartur are the least uraniferous but the highest in the REE budget.

The intercalated phosphorite beds and the highly silica facies represent the early transgressive stage, characterized by the dominance of detrital input [22]. Ref [23] assigned that the thickest deposits of phosphorite form in areas of geosynclinal subsidence, under reducing conditions, where phosphorite is associated with carbonaceous shale and chert, that usually carbonaceous, pelletal, and mixed with skeletal matter and phosphatic shells. The Duwi Formation was deposited at the initial stage of the late Cretaceous marine transgression in Egypt [13]. Beyond their role in fertilizer production, Egyptian phosphorites are enriched in trace and rare earth elements (REEs), offering additional strategic value for emerging technologies [16]. However, most previous studies have focused primarily on beneficiation and phosphoric acid production, with limited emphasis on the geochemical behavior and distribution of REEs [14,24].

Regionally, the Duwi Formation forms part of the extensive Tethyan Upper Cretaceous-Early Tertiary phosphogenic province that stretches across North Africa, the Middle East, and northern South America. In Egypt, the phosphorites occur as thin but widespread shallow-marine deposits forming an east–west belt across the mid-latitudes of the country. This province hosts one of the largest phosphorite accumulations globally, with estimated reserves exceeding 70 billion metric tons [25]. Within Egypt, the phosphorite belt extends from the Red Sea coast (El Qusseir-Safaga), through the Nile Valley (Idfu-Qena), and westward to the Abu Tartur region (Figure 1). The data of the present work, compared with other regions, together with previously published data, have collectively been integrated to conclude.

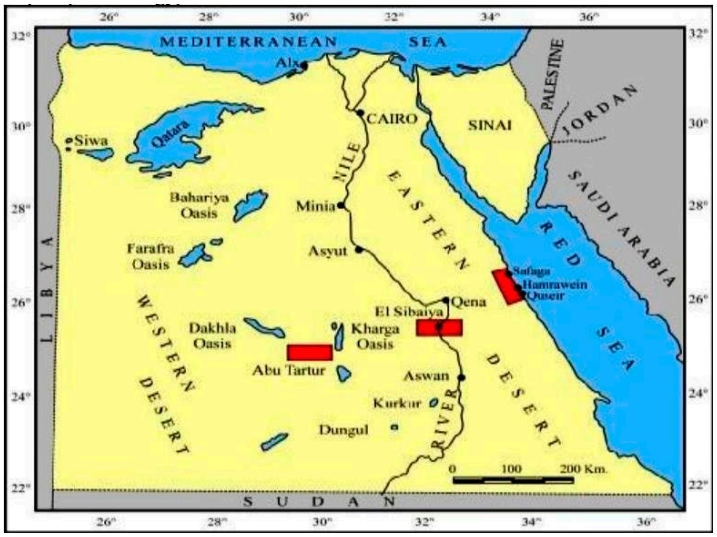

Figure 1. Location map of the phosphorite belt deposits in Egypt.

The investigated area covers approximately 310 km2, it's considered a part of the Nile Valley area, located between latitudes 25°15`00" and 25°20`00" North, and between longitudes 32°55`00" and 33°15`00" East, north of Idfu City in Aswan Governorate (Figure 2). This study examines five localities (e.g., Wadi Hilal, East Sibaiya, Um Higarah, Um Salama, and Um Tundbah), aiming to provide an integrated geological, petrographic, and geochemical assessment of the Upper Cretaceous

 doi:10.20944/preprints202603.0009.v1

phosphorites within this sector of the Nile Valley. Besides, study the distribution and abundance of REEs concentrations in the Egyptian phosphorites.

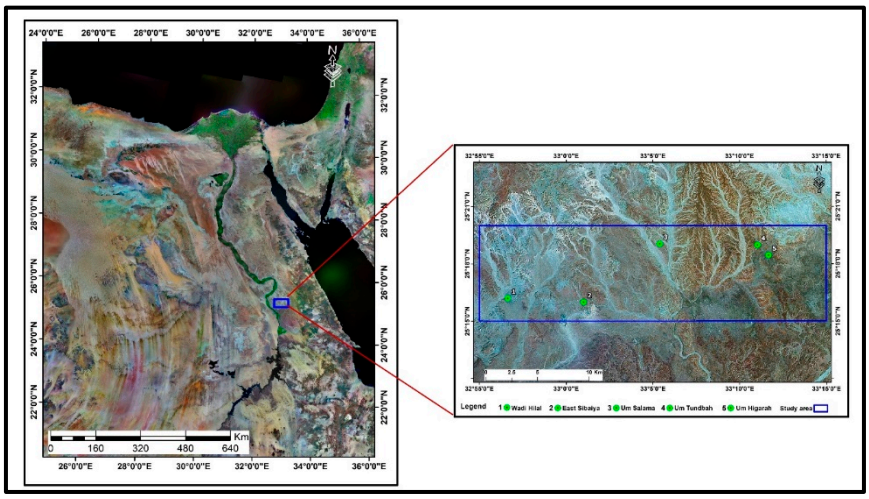

Figure 2. Key map showing the location map of the studied sections in North Aswan.

2. Materials and Methods

Thirty-six rock samples were collected from the Duwi Formation and the lower part of the Dakhla Formation at five localities: Wadi Hilal, East Sibaiya, Um Higarah, Um Salama, and Um Tundbah. These sites were selected to capture the full range of lithofacies observed within the studied stratigraphic intervals.

Twelve representative phosphate samples were prepared as standard thin sections for petrographic examination. Mineralogical composition and textural features were identified using a Nikon polarizing microscope equipped with an automated digital camera.

Sixteen phosphate samples were selected for major, trace, and rare earth elements (REEs) analyses. X-ray fluorescence (XRF) and inductively coupled plasma–mass spectrometry (ICP-MS) were performed at the GeoAnalytical Laboratory, Washington State University (WSU), USA. Sample preparation followed standard geochemical protocols. Each sample was crushed using a jaw crusher and pulverized in an agate grinding bowl to obtain a homogeneous fine powder. For XRF analysis, the powdered samples were fused with two parts di-lithium tetraborate flux at 1000 °C in a muffle furnace and allowed to cool. Loss on ignition (LOI) was determined from the mass difference after heating at 1000 °C. REE and selected trace-element concentrations were determined using an Agilent 7700 ICP-MS. Approximately 50 mg of each powdered sample was digested in acid-washed Teflon vessels with a 3:1 mixture of nitric and hydrofluoric acids and refluxed at 250 °C for at least 8 hours to ensure complete dissolution before analysis.

3. Geological Setting

Phosphorite deposits in Egypt belong to the Duwi Formation of Late Cretaceous (Campanian–Maastrichtian age). They are found in the Red Sea Coast, between Safaga - Qusseir area; Nile Valley between Idfu - Qena; Abu Tartur plateau in Western Desert, and Wadi Araba and Gebel Sofraiyat at Sinai Peninsula. The phosphatic deposits of this provenance are conformably overlain by gray, fine-grained, thinly layered fossiliferous marine shale of Paleocene Dakhla shale, and are overlain by non-marine, varicolored shale of the Santonian– Campanian Qusseir Formation [22].

The phosphatic succession of the Duwi Formation represents the establishment of the first fully marine conditions that spread across Egypt during the major Late Cretaceous transgression [26]. In the study area, the phosphorites occur along the eastern side of the Nile River. The formation consists mainly of phosphorite beds intercalated with shale, marl, oyster limestone, and chert. Five

 doi:10.20944/preprints202603.0009.v1

stratigraphic sections were logged, measured, and sampled at Wadi Hilal, East Sibaiya, Um Higarah, Um Salama, and Um Tundbah. The geological map, Figure 3, shows that most exposed units in the area belong to the Upper Cretaceous. The lithostratigraphic succession from base to top comprises the Qusseir Formation (Santonian–Campanian), the Duwi Formation (Campanian–Maastrichtian), and the Dakhla Formation (Paleocene), Figures 4 and 5.

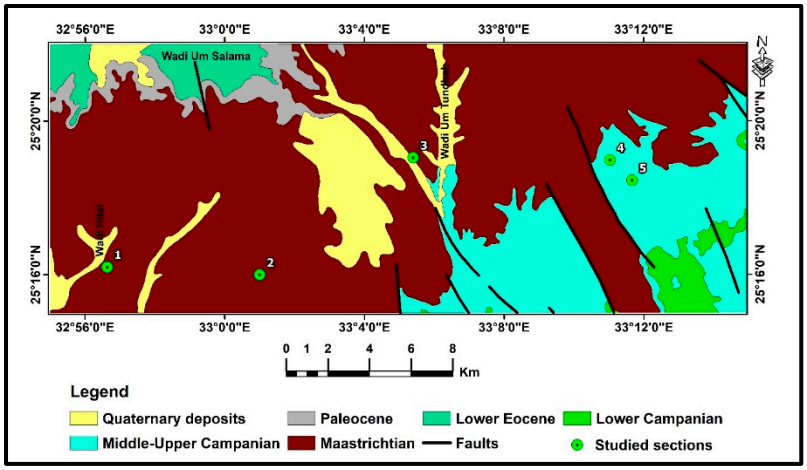

Figure 3. A geological map showing the rock units occurring in the study area (Modified after 59).

The Qusseir Formation was originally defined by [18] in the Qusseir district. It consists mainly of variegated shale with occasional sandstone interbeds. Ref. [19] Referred to the unit informally as the "Qusseir variegated shale," while [4] used the term "Qusseir shales," which has priority as the formal name. The Qusseir shales rest unconformably on the Nubia Sandstone and are overlain by the Duwi Formation. The variegated shale is characterized by Mg-rich minerals, such as smectite.

The term "Duwi Formation" was introduced by [18] for the phosphate-rich succession at Gebel El-Duwi in the Qusseir district. In the present study area, it forms a similar phosphate-bearing interval that overlies the Qusseir shale and is capped by the Dakhla shale. The formation is composed of oyster limestone, marl, chert, and phosphorite beds. Oyster limestone is brownish grey in color and a hard bed with a thickness of about 1.2 m. Marl is yellowish to yellowish grey in color, hard, cracked, and fractured bed with a thickness of about 2 m. Chert is a dark brown color and a very hard bed with a thickness of about 0.3 m. Phosphate is yellowish to brown in color, friable, with a total thickness of about 1.5 m Figure 5. Phosphorite is mainly composed of carbonate fluorapatite (Francolite) and is always cemented by secondary material such as silica, carbonates, and sulfates. There are two colors within the studied phosphorite samples: dark grey and yellowish brown colored.

Paleocene Dakhla shale conformably overlies the Duwi Formation. It is grey to dark grey, fissile, and soft to moderately hard. Its thickness varies between 5 and 12 m across the investigated localities Figure 5. Also, the shale interbedded that is related to this formation is characterized by Mg-bearing minerals such as smectite.

 doi:10.20944/preprints202603.0009.v1

Figure 4. Field photograph showing the studied Upper Cretaceous-Paleocene succession: a) lithostratigraphic succession at sibaiya area represent Duwi Formation overlaying the Qusseir Formation and underlying Dakhla Formation; b) phosphatic bed (A) at the lower part and phosphatic bed (B) at the upper part through the succession in Um Tundbah area; c) phosphate (B) bed in an open pit mine at Um Tundbah area; d) Duwi and Dakhla formations at Um Higarah area; e) intercalated between carbonate rocks with different phosphatic beds (A and B) at Um Higarah area; f) phosphate (A) bed at Um Salma area; g) chert band intercalated with phosphatic bed at Um Salma area; h) proper phosphatic bed confined between Oyster limestone and siliceous phosphatic bed at Wadi Hilal area; and i) Upper Cretaceous-Paleocene (Duwi and Dakhla formations) at Um Salma area.

 doi:10.20944/preprints202603.0009.v1

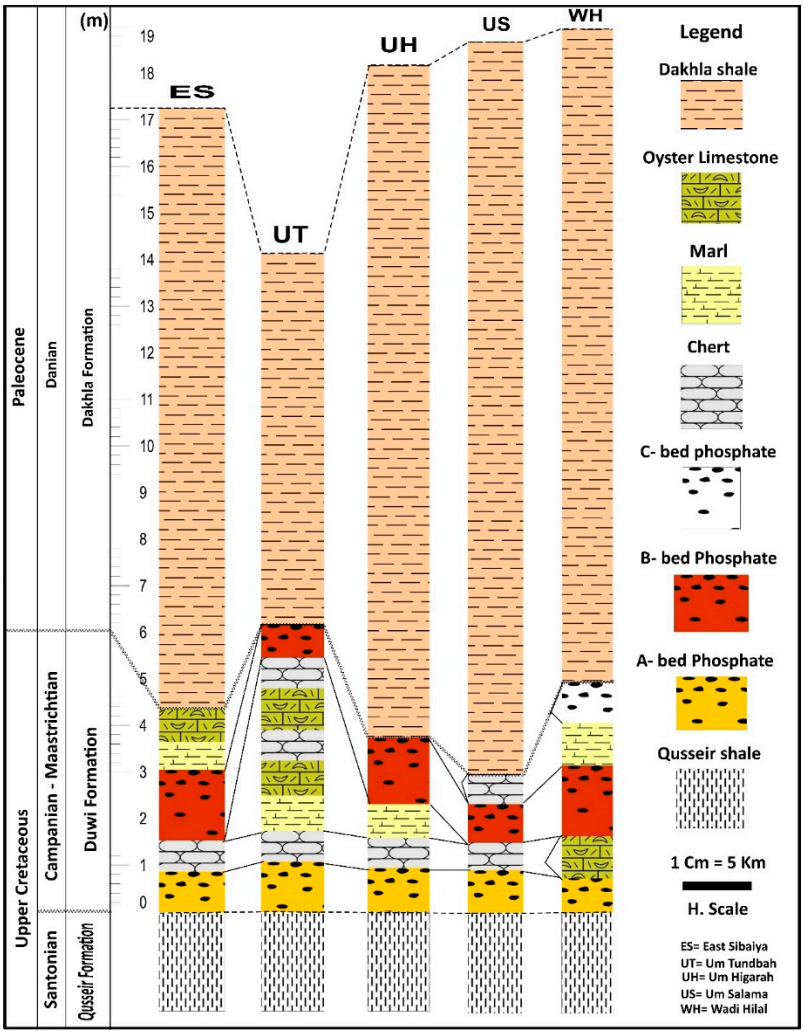

Figure 5. Lithostratigraphic columnar sections of the Upper Cretaceous-Paleocene sedimentary succession at East Sibaiya, Um Tundbah, Um Higara, Um Salma, and Wadi Hilal area.

4. Results

4.1. Field Description

The phosphatic-bearing beds of the Upper Cretaceous (Campanian) in the study area are exposed across five stratigraphic sections: Wadi Hilal, East Sibaiya, Um Higarah, Um Salama, and Um Tundbah. The regional lithostratigraphic succession, arranged from base to top, comprises the Qusseir Formation (Santonian–Campanian), the Duwi Formation (Campanian–Maastrichtian), and the Dakhla Formation (Paleocene). The Qusseir Formation consists predominantly of variegated shale, locally interbedded with thin sandstone layers. The shale exhibits distinctive reddish, greenish, and brownish colors, reflecting fluctuating oxidation conditions. Above this horizon lies the Duwi Formation, the principal phosphatic unit of the region. It conformably overlies the Qusseir shale and is conformably capped by the Dakhla shale. The Duwi Formation consists of phosphorite beds, marl, oyster limestone, and chert, with an overall thickness of approximately 5 m. The overlying Dakhla shale is composed of grey to dark-grey, fissile shale and ranges from 5 to 12 m in thickness across the study area.

At the Wadi Hilal area, it attain about 5m, it's composed of from base to top; low grad phosphatic (A bed; 50cm), Oyster limestone (1m), high-grade phosphatic with lenses from chert (B bed; 1.5m), silicified phosphate (20cm), intercalated between marl and oyster limestone (1.25cm), followed by phosphatic C-bed (50cm). These units are overlain by ~35 m of Dakhla shale Figure 5. The East Sibaiya section, the Duwi Formation, is ~4 m thick and is overlain by ~15 m of Dakhla shale. The sequence,

 doi:10.20944/preprints202603.0009.v1

from base to top, includes: high-grade phosphatic (50cm), silicified phosphate (30cm), low-grade phosphatic (1.20cm), silicified phosphate (40cm), chert (10cm), silicified limestone (50cm), marl (40cm); these layers are capped by an Oyster limestone bed (50cm) Figure 5.

Through the Um Higarah section, the Duwi Formation reaches a thickness of ~2.5 m and is capped by ~17 m of Dakhla shale. The sequence consists of: intercalated from phosphatic A-bed (90cm), high silicified phosphate and chert (40cm), marl (30cm), silicified phosphate (60cm), B-phosphatic bed (35cm), and capped by 17m of Dakhla shale Figure 5. The Um Tundbah section contains ~3.6 m of Duwi Formation, overlain by ~8 m of Dakhla shale. These are from base to top, phosphatic A-bed (50cm), intercalated with silicified phosphate (40cm), chert (1.10m), and marl (50cm), and followed by B-phosphatic bed (30cm) Figure 5. At the Um Salama section, the Duwi Formation reaches a thickness of ~2.5 m, followed by ~30 m of Dakhla shale. The Duwi sequence comprises: phosphatic A-bed (60cm), highly silicified phosphate (25cm), chert (30cm), siliceous phosphate (60cm), and is followed by a chert bed (70cm). The Um Salama section is capped by 30m of Dakhla shale Figure 5.

4.2. Mineralogical Composition

Petrographically, the studied phosphorite samples show that they are composed of phosphatic grains, non-phosphatic grains, and cement. These phosphatic grains are allochemical components modified from cryptocrystalline phosphorite mineral (collophane). The cryptocrystalline or amorphous material (collophane) that varies in color from yellow, brownish yellow to black, and it consists of pelloids (pellets), bioclasts, and bone fragments Figures 6a-c. Texturally, pellets may have different shapes and sizes. They may be well-rounded, sub-rounded, spherical, ovoid, irregular, or lath-shaped grains. Most of the pellets are well-rounded to sub-round in shape Figure 6d-e.

The phosphatic bioclasts are composed of bone fragments and shark teeth. They are angular to sub-angular, prismatic, or irregular in shape. Bone fragments are colorless and transparent under the binocular microscope. They show various shades of color, ranging from yellow to grey. They are generally anisotropic and show some lamellar twinning. Elongated and prismatic bone fragments show parallel extinction to the elongated axis Figure 6f. The non-phosphatic grains are composed mostly of quartz, which represents the most common form of silica, occurring as detrital grains that are angular to sub-angular, rounded to sub-round in shape, and silt to medium sand size grades. Cements are composed of silica, calcite, microcrystalline quartz, and iron oxide Figure 6g-h.

 doi:10.20944/preprints202603.0009.v1

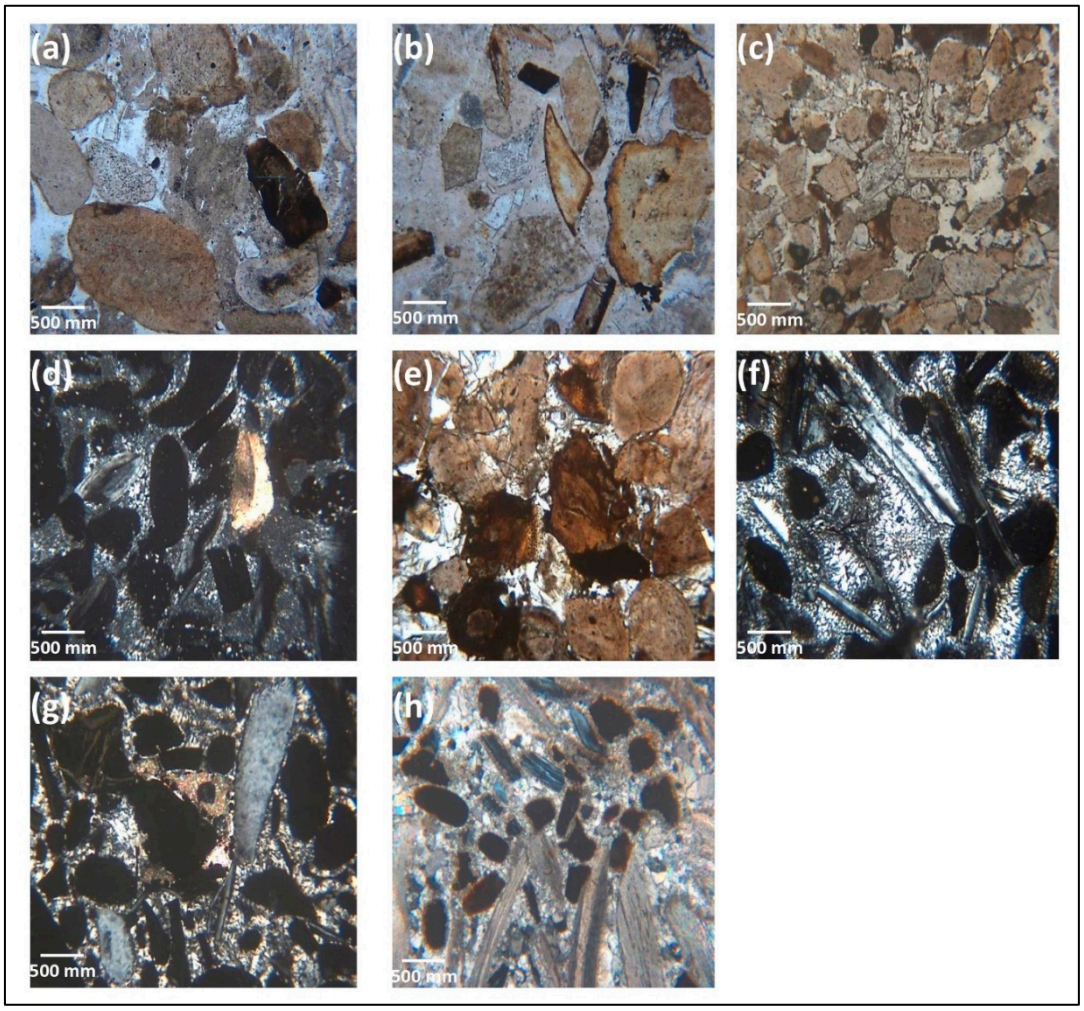

Figure 6. Photomicrograph showing different constituents of the studied phosphorites: a) photomicrograph showing collophane (brown grains) replaced by secondary silica (silicification), Um Tundbah-2, (63X, PPL); b) photomicrograph showing phosphatic collophane grains (brown grains) and phosphatic bioclasts (shark teeth) embedded in silica cement, Um Salma -2, (25X, PPL); c) Photomicrograph showing sub rounded yellowish to brown collophane grains embedded in silica cement, East Sibaiya -1, (25X, PPL); d) photomicrograph showing collophane grains and phosphatic bioclasts (bone fragments and shark teeth) embedded in microcrystalline quartz cement, Um Higarah-3, (25X, C.N); e) photomicrograph showing collophane of colloform texture with rare iron oxides embedded in calcite cement, Um Tundbah-1, (25X, C.N.); f) photomicrograph showing phosphatic bioclasts; bone fragments embedded in microcrystalline quartz cement, Um Higarah-2, (63X, C.N.); g) photomicrograph collophane grains and phosphatic bioclasts (bone fragments) embedded in microcrystalline quartz cement, Wadi Hilal-4, (25X, C.N.); and h) photomicrograph showing collophane grains and phosphatic bioclasts (microfossils, fossil shells) and pelloids that are scattered in the matrix of fine to medium-grained calcite (sparite), East Sibaiya -2, (25X, C.N.).

4.3. Whole-Rock Geochemistry

The geochemical distribution of the major oxides and trace elements gives direct information on the depositional environment. The major elements, which are located within the apatite lattice and include CaO, P_2O_5, F, CO_2, and Na_2O. On the contrary, the trace elements, which are located outside the apatite lattice and include SiO_2, Al_2O_3, and K_2O, whereas the other components, such as MgO, MnO, and Fe_2O_3, are introduced to the phosphorites by the weathering process. These elements may be associated with detrital minerals, organic matter, and may also be introduced by weathering processes.

 doi:10.20944/preprints202603.0009.v1

4.3.1. Major Elements

The main elemental compositions of the phosphatic deposits are CaO and P_2O_5, and it shows a significant positive correlation between them (Tables 1 and 2). The CaO content ranges from 26.91 to 52.78% (with an average of 40.97%). The P_2O_5 content ranges from 17.4 to 31.24% (with an average of 23.72%). The MgO content ranges from 0.23 to 0.56% (with an average of 0.33%). The SiO_2 content ranges from 2.48 to 47.67 (with an average of 20.95%). The Al_2O_3 content ranges from 0.13 to 1.84% (with an average of 0.53%). The Fe_2O_3 content ranges from 0.66 to 2.33% (with an average of 1.49%). The fluorine (F) content ranges from 0.14 to 1.73 % (with an average of 1.30%). The chlorine (Cl) content ranges from 0.01 to 1.16% (with an average of 0.20%). The concentration values of Ti, Mn, and Mg are very low, whereas the Na and K contents are also illustrated in Table 1.

The CaO gives the strong positive relationships between L.O.I and P_2O_5 (r = 0.70 and 0.74, respectively) Figure 7a-b; Table 2. The CaO gives the strong negative relationships between SiO_2 and Sr (r = -0.98 and -0.61, respectively) Figure 7c-d. CaO/P_2O_5 ratios range from 1.56% to 2.12% (with an average of 1.76%, Table 1). SiO_2 gives a strong negative correlation with Sr and L.O.I (r = -0.71 and -0.72, respectively), Figure 7e-f. P_2O_5 shows strong negative relationships with SiO_2 (r = -0.72), Figure 7g; Table 2, whereas it gives very weak positive correlations between Fe_2O_3, F, and S (r = 0.11, 0.17, and 0.23, respectively). On the other hand, P_2O_5 gives a medium negative correlation between TiO_2, Al_2O_3, and K_2O (r = - 0.48, - 0.43, and - 0.46, respectively); Table 2. P_2O_5 also shows very weak negative relationships with MgO and Cl (r = - 0.16 and - 0.06, respectively). Zr shows the strong positive correlation with SO3 (r = 0.82), Figure 7h, whereas Zr gives the strong negative correlation with SiO_2 (r = - 0.73), Figure 7j. Al_2O_3 represents a very strong positive correlation with TiO_2 and K_2O (r = 0.98 and 0.95, respectively), Figure 7i - k; Table 2.

Table 1. XRF analysis showing the major oxides (wt. %) and trace elements (ppm) of the studied phosphatic rock samples.

Area	Wadi Hilal					East Sibaiya			Um Higara					Um Salama				Um Tundbah				Total
Sample	1	3	4	6	Aver.	1	3	Aver.	1	2	5	6	Aver.	1	2	4	Aver.	1	2	6	Aver.	average
SiO_2	4.25	5.93	33.89	22.63	16.68	4.66	10.85	7.76	2.71	34.77	47.67	26.1	27.81	4.11	36.63	33.42	24.72	2.48	34.53	30.6	22.54	20.95
TiO_2	0.01	0.01	0.01	0.07	0.02	0.01	0.01	0.01	0.01	0.01	0.05	0.03	0.02	0.01	0.01	0.02	0.01	0.01	00.1	0.07	0.02	0.02
Al_2O_3	0.19	0.29	0.19	1.83	0.63	0.27	0.24	0.26	0.14	0.29	1.08	0.92	0.61	0.18	0.22	0.52	0.31	0.13	0.13	1.84	0.70	0.53
Fe_2O_3	1.59	2.14	1.53	2.33	1.90	1.45	1.04	1.25	0.86	0.87	0.66	2.24	1.16	1.87	1.45	1.72	1.68	1.1	0.84	2.08	1.34	1.49
MgO	0.33	0.39	0.3	0.56	0.40	0.34	0.33	0.34	0.3	0.27	0.32	0.35	0.31	0.31	0.28	0.28	0.29	0.28	0.23	0.44	0.32	0.33
CaO	48.98	46.82	33.84	37.02	41.67	49.96	47.6	48.78	52.78	36.33	26.91	37.35	38.34	49.87	32.94	34.49	39.10	52.07	34.65	33.85	40.19	40.97
Na_2O	0.6	1.2	0.89	1.41	1.03	0.69	0.53	0.61	0.41	0.46	0.49	0.59	0.49	0.72	0.58	0.57	0.62	0.41	0.4	0.62	0.48	0.66
K2O	0.01	0.02	0.02	0.1	0.04	0.01	0.01	0.01	0.01	0.02	0.06	0.05	0.03	0.02	0.02	0.04	0.03	0.01	0.01	0.07	0.03	0.03
P_2O_5	21.22	28.23	21.36	20.92	22.93	26.54	19.46	23.00	29.22	23.22	17.4	23.11	23.24	31.24	21.47	22.43	25.05	29.79	22.41	21.47	24.56	23.72
MnO	0.11	0.1	0.1	0.09	0.10	0.07	0.06	0.07	0.06	0.09	0.05	0.09	0.07	0.07	0.09	0.06	0.07	0.07	0.07	0.07	0.07	0.08
F	1.22	1.36	1.46	0.98	1.26	0.14	1.16	0.65	1.53	1.48	1.25	1.31	1.39	1.55	1.46	1.46	1.49	1.73	1.55	1.14	1.47	1.30
Cl	0.22	0.87	0.44	1.16	0.67	0.11	0.10	0.11	0.02	0.02	0.03	0.04	0.03	0.02	0.02	0.01	0.02	0.01	0.01	0.12	0.05	0.20
S	1.52	2.14	0.99	1.11	1.44	0.10	0.45	0.28	0.24	0.25	0.21	0.29	0.25	1.52	0.43	0.37	0.77	0.21	0.21	0.34	0.25	0.65
LOI	16.62	7.71	5.29	9.64	9.82	12.39	17.61	15.00	11.02	1.37	4.16	6.77	5.83	6.17	4.65	4.71	5.18	10.17	4.6	6.04	6.94	8.06
Cr	104.43	113.43	161.37	76.93	114.04	89.75	110.83	100.29	122.15	136.56	164.09	107.55	132.59	107.18	172.74	112.19	130.70	104.98	171.93	117.29	131.40	123.34
Ni	26.65	32.54	19.9	53.12	33.05	19.4	15.09	17.25	20.33	18.89	10.99	37.86	22.02	39.82	23.15	27.72	30.23	23.37	10.27	81.1	38.25	28.76
Cu	15.82	13.91	17.48	15.12	15.58	12.62	17.28	14.95	15.82	13.23	11.72	12.81	13.40	20.45	13.62	14.39	16.15	11.7	12.86	22.23	15.60	15.07
Zn	187.33	266.45	138.21	247.76	209.94	175.81	131.79	153.80	178.68	184.55	164.23	206.82	183.57	279.14	204.44	246.91	243.50	247.53	184.54	280.49	237.52	207.79
Sr	2281.44	2675.3	1703.01	2442.22	2275.49	1855.98	1695.39	1775.69	1811.86	1285.7	1237.11	1535.19	1467.47	2225.98	1378.25	1447.27	1683.83	1784.85	1292.11	1338.57	1471.84	1749.39
Zr	199.8	228.96	142.79	209.43	195.25	164.26	149.31	156.79	155.86	109.94	106.21	137.43	127.36	189.09	117.56	124.17	143.61	153.27	108.31	125.82	129.13	151.39
Ba	702.05	827.9	433.4	1920.91	971.07	733.35	491.73	612.54	655.38	372.97	361.54	328.22	429.53	597.64	326.33	327.21	417.06	754.07	441.89	268.6	488.19	596.45
V	90.89	156.65	172.78	82.11	125.61	112.43	68.16	90.30	199.01	281.43	0.01	0.01	120.11	208.32	254.19	286.66	249.72	322.82	462.7	121.06	302.19	176.20
Pb	5.96	6.29	6.11	4.64	5.75	3.59	2.58	3.09	3.6	4.86	4.49	4.49	4.36	6.37	9.36	12.26	9.33	4.9	5.62	6.19	5.57	5.71
Th	1.73	1.92	1.23	1.86	1.69	1.11	0.77	0.94	0.8	1.07	1.36	2.25	1.37	1.05	1.25	4.07	2.12	0.61	0.74	3.3	1.55	1.57
U	68.89	111.85	123.37	50.62	88.68	89.28	40.59	64.94	144.46	173.63	181.11	63.94	140.79	136.64	166.48	204.73	169.28	181	245.84	64.61	163.82	127.94
Cao/P_2O_5	2.31	1.66	1.58	1.77	1.82	1.88	2.45	2.12	1.81	1.56	1.55	1.62	1.65	1.60	1.53	1.54	1.56	1.75	1.55	1.58	1.64	1.76
Th/U	0.03	0.02	0.01	0.04	0.02	0.01	0.02	0.01	0.01	0.01	0.01	0.04	0.01	0.01	0.01	0.02	0.01	0.00	0.00	0.05	0.01	0.02

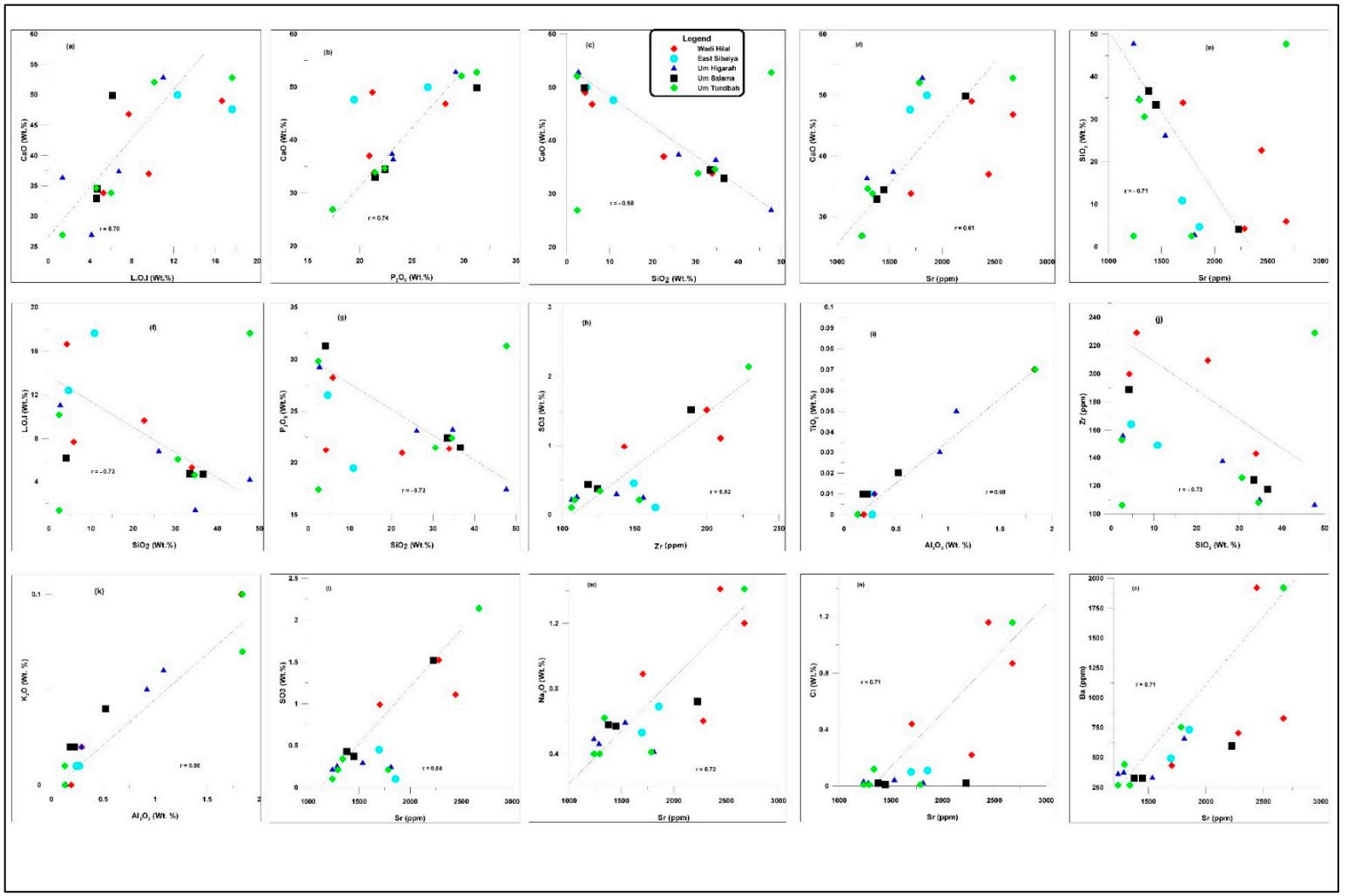

Figure 7. Inter-elemental relationships between major oxides (wt. %) and trace elements (ppm) in the phosphorite of the studied area.

 doi:10.20944/preprints202603.0009.v1

4.3.2. Trace and Radioactive Elements

The trace element content in the phosphatic rock samples is given in Table 1. The results showed that the studied phosphorites are enriched in Sr, Ba, Zn, Zr, Cr, V, and Ni with low contents of Cu and Pb. The Sr content varies from 1237.11 to 2675.3 ppm, with an average of 1749.39 ppm. The Sr shows a strong positive correlation between Ba, Cl, Na, and S (r = 0.71, 0.71, 0.72, and 0.84, respectively), Figure 7l-o, whereas give a moderate positive relationship with P_2O_5, Fe_2O_3, MgO, MnO, and L.O.I (r = 0.45, 0.53, 0.51, 0.46, and 0.49, respectively). On the other hand, Sr represents a moderately negative correlation with Cr (r = - 0.62; Figure 8a), whereas it shows no relationship between Ti, Al, K, and F (r = - 0.05, - 0.05, -0.03, and – 0.16, respectively) Table 2.

The Ba content ranges from 268.6 to 1920.91 ppm with an average of 596.45 ppm. It shows a strong positive correlation between Mg, Na, Cl, Sr, and Zr (r = 0.71, 0.73, 0.80, 0.71, and 0.70, respectively, Figure 8b-f, whereas give a moderate to weak positive relationship with Ti, Al, Fe, Ca, K, P_2O_5, Mn, S, L.O.I., Ni, and Zn. On the other hand, Ba represents a moderately to weak negative correlation with Si, F, Cr, and Cu Table 2. The Zn content ranges from 131.79 to 280.49ppm (with an average of 207.79ppm) Table 1. The Zn shows a strong positive relationship with Fe and Ni (r = 0.63 and 0.72, respectively; Figure 8g-h, and gives a weak positive relationship with other elements Table 2. Ni content ranges from 10.27 to 81.1 ppm Table 1, with an average of 28.76 ppm. The Ni shows a strong positive relationship with Ti, Al, Fe, Mg, and k (r = 0.71, 0.75, 0.76, 0.72, and 0.63, respectively; Figure 8i-m), whereas it gives a weak negative relationship with Si, Ca, F, and L.O.I. (Table 2).

The V content ranges from 0 to 462.7 ppm (with an average of 176.20ppm). The V shows a weak positive relationship with P_2O_5 (r = 0.34), whereas it gives a moderately negative correlation with Ti, Al, Mg, and F (r = -0.50, -0.48, -0.58, and -0.50, respectively; Table 2). The Zr content ranges from 106.21 to 228.96 ppm (with an average of 151.39ppm) Table 1. The Zr shows a moderate to strong positive relationship with Fe, Mg, Ca, Ns, P, Mn, Cl, and S (r = 0.56, 0.55, 0.62, 0.71, 0.43, 0.45, 0.71, 0.82, and 0.52, respectively; Figure 8n), whereas give strong negative correlation with Si (r = - 0.73, Figure 7j), and Cr (r = -0.67; Figure 8o, Table 2). The Cr content ranges from 76.93 to 172.74 ppm (with an average of 123.34ppm). It's shown the moderately positive correlation with Si and F (r = 0.67 and 0.44, respectively). On the other hand, Cr shows a weak negative correlation with the P_2O_5, Fe, Mg, Ca, Na, and Cl (r = - 0.36, -0.54, -0.59, -0.60, -0.39, and -0.36, respectively) Table 2.

The geochemical analysis of the radioactive elements (U and Th) in the studied phosphatic rock samples is listed in Table 1. The U shows a strong positive relationship with F, Cr, and V (r = 0.53, 0.62, and 0.77, respectively), whereas it gives a very weak positive relationship with P_2O_5 (r = 0.14; Table 2). Besides, it also shows a moderate to weak negative relationship with CaO, Ti, Mg, Fe, Na, Cl, S, and L.O.I (r = -0.27, -0.38, -0.71, -0.57, -0.47, -0.43, -0.31, and -0.61, respectively). U represent a very weak negative relationship with Th (r = - 0.14) Table 2. Th/U ratios range from 0.00% to 0.05% (with an average of 0.02%, Table 1).

Table 2. Pearson correlation coefficient of the phosphatic rock samples in the study area.

	SiO_2	TiO_2	Al_2O_3	Fe_2O_3	MgO	CaO	Na_2O	K_2O	P_2O_5	MnO	F	Cl	S	LOI	Cr	Ni	Cu	Zn	Sr	Zr	Ba	V	Pb	Th	U
SiO_2	1.00																								
TiO_2	0.40	1.00																							
Al_2O_3	0.37	0.98	1.00																						
Fe_2O_3	-0.16	0.44	0.49	1.00																					
MgO	-0.11	0.77	0.80	0.69	1.00																				
CaO	-0.98	-0.51	-0.49	0.00	-0.04	1.00																			
Na2O	-0.12	0.38	0.40	0.71	0.77	-0.03	1.00																		
K_2O	0.49	0.94	0.95	0.52	0.75	-0.61	0.51	1.00																	
P_2O_5	-0.72	-0.48	-0.43	0.11	-0.16	0.74	0.00	-0.46	1.00																
MnO	-0.09	-0.10	-0.08	0.48	0.22	0.02	0.49	-0.05	-0.03	1.00															
F	0.16	-0.21	-0.28	-0.21	-0.44	-0.10	-0.29	-0.21	0.17	0.03	1.00														
Cl	-0.12	0.37	0.40	0.57	0.77	-0.01	0.95	0.47	-0.06	0.50	-0.21	1.00													
S	-0.38	-0.02	-0.07	0.54	0.35	0.27	0.69	0.00	0.23	0.60	0.10	0.64	1.00												
LOI	-0.72	-0.17	-0.16	0.02	0.22	0.70	0.05	-0.31	0.06	0.03	-0.38	0.13	0.17	1.00											
Cr	0.67	-0.22	-0.27	-0.54	-0.59	-0.60	-0.39	-0.19	-0.36	-0.06	0.44	-0.36	-0.25	-0.56	1.00										
Ni	-0.04	0.71	0.75	0.76	0.72	-0.09	0.41	0.63	0.04	0.15	-0.13	0.33	0.23	-0.07	-0.45	1.00									
Cu	-0.15	0.27	0.26	0.37	0.31	0.10	0.16	0.16	0.05	0.00	0.04	0.06	0.32	0.12	-0.17	0.64	1.00								
Zn	-0.19	0.38	0.37	0.63	0.40	0.10	0.34	0.36	0.46	0.05	0.17	0.24	0.36	-0.24	-0.41	0.72	0.29	1.00							
Sr	-0.71	-0.05	-0.05	0.53	0.51	0.61	0.72	-0.03	0.45	0.46	-0.16	0.71	0.84	0.49	-0.62	0.21	0.16	0.35	1.00						
Zr	-0.73	-0.01	0.00	0.56	0.55	0.62	0.71	-0.01	0.43	0.45	-0.21	0.70	0.82	0.52	-0.67	0.27	0.19	0.37	1.00	1.00					
Ba	-0.37	0.30	0.33	0.37	0.71	0.27	0.73	0.36	0.13	0.24	-0.28	0.80	0.39	0.34	-0.59	0.23	-0.07	0.24	0.71	0.70	1.00				
V	0.06	-0.50	-0.48	-0.35	-0.58	0.02	-0.32	-0.44	0.34	-0.08	0.50	-0.27	-0.17	-0.37	0.37	-0.27	-0.15	0.15	-0.24	-0.29	-0.17	1.00			
Pb	0.35	0.01	-0.04	0.27	-0.20	-0.37	0.03	0.09	-0.06	0.10	0.32	-0.08	0.13	-0.45	0.22	0.13	0.05	0.41	-0.14	-0.16	-0.26	0.39	1.00		
Th	0.30	0.54	0.54	0.59	0.34	-0.39	0.21	0.55	-0.26	0.02	-0.08	0.12	0.07	-0.23	-0.24	0.59	0.26	0.49	-0.08	-0.04	-0.12	-0.18	0.63	1.00	
U	0.38	-0.38	-0.41	-0.57	-0.71	-0.27	-0.47	-0.29	0.14	-0.32	0.53	-0.43	-0.31	-0.61	0.62	-0.51	-0.43	0.00	-0.47	-0.53	-0.36	0.77	0.43	-0.14	1.00

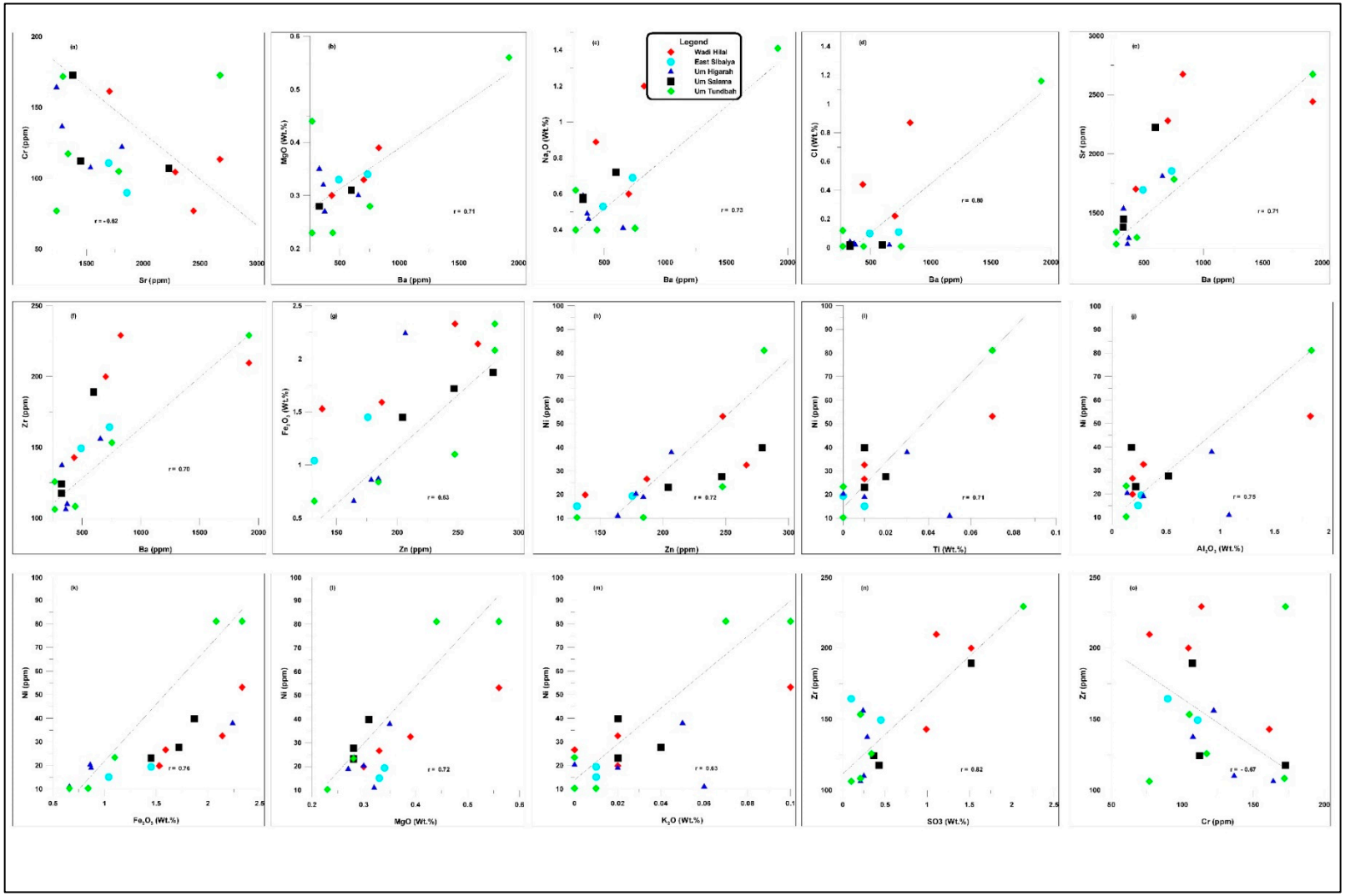

Figure 8. Inter-elemental relationships between major oxides (wt. %) and trace elements (ppm) in the phosphorite of the studied area.4.3.3. Rare Earth Elements (REEs).

 doi:10.20944/preprints202603.0009.v1

The rare earth elements concentration in the studied phosphorite samples is shown in Table 3. The total rare earth elements (∑REEs) contents range from 47.83 to 270.37 ppm (with an average of 146.19 ppm). The light rare earth elements (LREEs) represent more than 85% of the total rare earth elements in the studied phosphorites, with contents ranging from 39.41 to 233.69 ppm (with an average of 123.74ppm). The heavy rare earth elements (HREEs) show less than 15% of the total rare earth elements, with contents ranging between 7.87 to 38.52ppm (with an average of 22.45ppm), Table 3. Ce/La ratios in the present work vary from 1.14 to 1.75 (with an average of 1.51), whereas the Eu/Eu* ratios range from 0.76 to 0.81 (with an average of 0.79), Table 3.

Table 3. REEs concentrations (ppm) in the studied phosphorite samples.

Samples No.		WH 1	WH 3	WH 4	WH 6	Aver.	ES 1	ES 3	Aver.	UH 1	UH 2	UH 5	UH 6	Aver.	US 1	US 2	US 4	Aver.	UT 1	UT 2	UT 6	Aver.
LREEs	La	42.53	52.49	38.55	30.71	41.07	27.04	14.37	20.71	18.29	21.76	11.62	33.66	21.33	33.68	43.59	61	46.09	21.34	25.54	47.46	31.45
	Ce	70.97	82.77	56.62	50.94	65.33	42.88	25.2	34.04	25.8	35.29	14.52	58.77	33.6	47.45	64.09	97.93	69.82	24.32	30.02	76.68	43.67
	Pr	9.11	10.8	7.53	6.18	8.405	5.56	3.29	4.425	3.75	4.99	2.24	7.65	4.658	6.23	8.42	12.5	9.05	3.56	4.39	9.93	5.96
	Nd	37.87	45.11	31.54	26.36	35.22	23.36	13.57	18.47	15.58	20.18	8.81	30.89	18.87	25.82	33.9	49.98	36.57	14.79	18.35	40.12	24.42
	Sm	7.34	9.08	6.35	5.17	6.985	4.49	2.7	3.595	3.07	4.04	1.75	6.36	3.805	5.12	6.64	9.84	7.20	2.94	3.55	8.04	4.843
	Eu	2.1	2.47	1.77	1.55	1.973	1.22	0.69	0.955	0.81	1.06	0.47	1.68	1.005	1.28	1.69	2.44	1.80	0.79	0.94	2.15	1.293
HREEs	Gd	8.2	10.2	7.41	6.38	8.048	5.06	2.26	3.66	3.73	4.53	1.75	6.52	4.133	5.28	6.74	9.86	7.29	3.4	4.02	8.15	5.19
	Tb	1.24	1.45	1.04	0.92	1.163	0.74	0.37	0.555	0.55	0.68	0.3	0.94	0.618	0.79	1.02	1.39	1.07	0.51	0.6	1.19	0.767
	Dy	7.86	9.78	6.91	5.78	7.583	4.91	2.08	3.495	3.7	4.45	2.04	6.01	4.05	5.18	6.62	9.22	7.01	3.32	4.17	7.55	5.013
	Ho	1.77	2.21	1.59	1.29	1.715	1.15	0.44	0.795	0.85	1.07	0.54	1.34	0.95	1.23	1.52	2.11	1.62	0.82	1.04	1.72	1.193
	Er	5.3	6.69	4.83	3.77	5.148	3.51	1.2	2.355	2.73	3.41	1.71	4.13	2.995	3.8	4.8	6.38	4.99	2.5	3.3	5.17	3.657
	Tm	0.74	0.94	0.66	0.56	0.725	0.49	0.17	0.33	0.37	0.46	0.23	0.55	0.403	0.52	0.67	0.87	0.69	0.34	0.47	0.72	0.51
	Yb	5.12	6.25	4.62	3.75	4.935	3.31	1.18	2.245	2.62	3.17	1.6	3.87	2.815	3.63	4.67	5.92	4.74	2.44	3.15	4.99	3.527
	Lu	0.79	1	0.73	0.58	0.775	0.54	0.17	0.355	0.41	0.48	0.25	0.6	0.435	0.58	0.75	0.92	0.75	0.39	0.5	0.75	0.547
∑LREEs		169.9	202.7	142.4	120.9	159	104.6	59.82	82.19	67.3	87.32	39.41	139	83.26	119.6	158.3	233.69	170.53	67.74	82.79	184.4	111.6
∑HREEs		31.02	38.52	27.79	23.03	30.09	19.71	7.87	13.79	14.96	18.25	8.42	23.96	16.4	21.01	26.79	36.67	28.157	13.72	17.25	30.24	20.4
∑REEs		200.9	241.2	170.2	143.9	189.1	124.3	67.69	95.98	82.26	105.6	47.83	163	99.66	140.6	185.1	270.36	198.69	81.46	100.04	214.6	132
Ce/La		1.669	1.577	1.469	1.659	1.591	1.586	1.754	1.644	1.411	1.622	1.25	1.746	1.575	1.409	1.47	1.6054	1.5149	1.1396	1.1754	1.616	1.389
Eu/Eu*				0.8				0.81				0.78					0.76				0.79	

 doi:10.20944/preprints202603.0009.v1

5. Discussion

5.1. Lithostratigraphic Positions

The Qusseir variegated shale typically displays reddish, greenish, and brownish colors, reflecting periodic fluctuations in oxidation conditions. Its dominance within the succession indicates deposition in low-energy coastal to delta-plain settings, with intermittent suboxic to oxic conditions. Occasional sandstone beds reflect episodic influxes of clastic sediments, likely associated with fluvial or deltaic progradation. Periodic shifts in oxidation state suggest shifts between restricted lagoonal conditions and more open coastal settings. Furthermore, the Qusseir Formation records a transgressive–regressive cycle marking the transition from continental siliciclastic sedimentation toward increasingly marine conditions before the major Campanian–Maastrichtian transgression. The unit unconformably overlies the Nubia Sandstone and represents the shift from continental to shallow-marine environments.

According to [27], the formation of Mg-rich shale (smectite mineral) after periods of phosphorite deposition seems to be a necessity to normalize the sharp increase in Mg relative to Ca. As a result of burial diagenesis of the Mg-rich clays and their transformation into more stable illite, the released Mg, Fe, and silica are directly responsible for the ferroan-dolomitization of the carbonate interbeds and cementation of phosphorite by silica [28,29]. The phosphatic succession of the Duwi Formation was formed under oscillating regimes controlled by relative sea-level rise during the Late Cretaceous global transgression. High marine productivity supplied abundant biogenic apatite, while periodic anoxia at the sediment–water interface promotes phosphate concentration. Reworking processes, pelletization, winnowing, and redistribution play a key role in shaping the phosphatic texture.

The associated oyster limestone reflects deposition in shallow, oxygenated, open-marine conditions, where bivalves thrived on a stable carbonate shelf. Marl units reflect a quieter, moderately deep, low-energy shelf environment, with increased clay input and reduced carbonate productivity. Chert horizons indicate silicification linked to upwelling-influenced waters with high planktonic silica productivity, consistent with nutrients-rich transgressive water. Phosphorite beds formed under upwelling-controlled, nutrient-rich conditions, with fluctuating redox states ranging from suboxic to anoxic. Reworking by waves and currents, forming pellets and conglomeratic textures, while condensed sedimentation favored phosphate accumulation. Obviously, the Duwi Formation reflects deposition on a shallow epicontinental shelf influenced by upwelling, high productivity, and episodic oxygen depletion, ideal conditions for phosphorite genesis. The dark colored of phosphorites samples are related to the presence of organic matter and/or sulfides, while the bright colors result from diagenetic or weathering processes.

The overlying Dakhla Formation, composed mainly of fine-grained, fissile shale, indicates deeper, low-energy offshore deposition. Its dark coloration suggests increased organic matter preserved under dysoxic bottom-water conditions. This unit marks the shift from phosphate-rich shallow shelf environments to a more open-marine basin during the early Paleocene. The Dakhla shale records the maximum flooding following the Campanian–Maastrichtian marine transgression.

5.2. Petrographic Characteristics

Petrographically, the phosphorites indicate deposition in a shallow-marine, nearshore shelf environment with high biogenic productivity, as suggested by abundant pellets and skeletal fragments. The variable energy conditions are inferred from pellet rounding, bioclast preservation, and intercalated fine sediments. Low sedimentation rates favor condensed phosphogenesis, while periodic influx is indicated by quartz grains of varying shape and size. Also, early diagenetic cementation stabilizes the phosphatic framework under suboxic to oxic conditions. In other words, these features (mineralogy and textures) support deposition on a shallow epicontinental shelf, influenced by biogenic accumulation, winnowing, and episodic reworking, conducive to forming economically important phosphorite beds.

 doi:10.20944/preprints202603.0009.v1

The phosphatic grains are allochemical components derived from cryptocrystalline phosphorite (collophane). According to [30], the amorphous grains (peloids) formed through algal micritization of skeletal debris represent primary biogenic material. Collophane displays colors from yellow and brownish-yellow to black and includes peloids (pellets), bioclasts, and bone fragments. Pellets exhibit diverse morphology, including well-rounded, sub-rounded, spherical, ovoid, irregular, and lath-shaped. Their predominantly rounded nature suggests moderate transport and reworking under low- to moderate-energy conditions. The presence of pelletized phosphorite suggests condensed sedimentation in a shallow marine shelf, where winnowing and periodic currents reworked biogenic material. Phosphatic bioclasts, including bone fragments and shark teeth, are angular to sub-angular and display prismatic or irregular shapes. Bone fragments are colorless and transparent under binocular examination, but show yellow to grey shades petrographically. They are anisotropic with lamellar twinning, and prismatic fragments exhibit parallel extinction. These features indicate minimal transport, rapid burial, and preservation in oxygen-deficient bottom waters.

Non-phosphatic grains are dominated by quartz, occurring as angular to sub-angular, or rounded to sub-rounded grains, ranging from silt to medium sand size. Their detrital nature indicates periodic terrigenous input from nearby landmasses or riverine influx systems, consistent with deposition in a proximally influenced shallow-marine environment. The cementing material comprises silica, calcite, microcrystalline quartz, and iron oxides, indicating early diagenetic processes under suboxic to oxic conditions that stabilized the phosphatic framework. Silica-rich cements may reflect siliceous water conditions influenced by upwelling and biogenic silica supply. These characteristics confirm deposition in shallow marine conditions near shore settings. The similarity in texture and composition is related to depositional environments on a global scale.

5.3. Geochemical Implications

Geochemical characteristics revealed that the silica is mainly detrital quartz, and microcrystalline silica also occurs as cement, chert bands, and free silica. Silicon may substitute for phosphorus in the apatite [31]. Alkali metals such as K_2O likely represent traces of trapped seawater during deposition. Variation in Fe_2O_3 reflects the diagenetic alteration. Ref. [32] Noted that the Egyptian phosphorites were initially deposited under a reducing environment (grey to black) and later oxidized to yellowish-brown during oxidation by chemical weathering. The low Fe_2O_3 content of the studied phosphate indicates the formation of phosphate in the near-surface oxidizing environment [24].

The low MgO content indicates limited dolomitization, whereas TiO_2 likely reflects detrital heavy minerals such as rutile and anatase. The low average content of Al_2O_3, Fe_2O_3, and MgO indicates that the studied phosphates precipitated in sedimentary basins and the formation of phosphate in the near-surface oxidizing environment, that match with [14,33]. Fluorine is incorporated within the apatite lattice, either freely or associated with the hydroxyl and oxygen ions [34]. Chlorine may be substituted for hydroxyl or fluorine in apatite or be associated with fine-grained clay minerals [35].

The high average silica content (20.95%) is an indication of biogenic origin [23]. The strong negative correlation between SiO_2 and P_2O_5 (r= -0.72) is related to the detrital quartz. The very strong positive correlation between Al_2O_3 and TiO_2 (r= 0.98) indicates enrichment of the immobile elements during the chemical weathering condition, and these elements are adsorbed on the surface of the clay mineral and associated with fine particles.

The negative correlation between SiO_2 and P_2O_5 is related to the detrital quartz. Strong positive correlation between P_2O_5 and CaO indicates the presence of calcite cement, that consistent with [36]. Negative correlation indicates elements located outside the apatite lattice and a result of later diagenesis. CaO/P_2O_5 in the fossil fish teeth varied in the range of 1.19 to 1.39, while CaO/P_2O_5 in the modern fish teeth varied in the range of 1.00 to 1.27. The value of CaO/P_2O_5 ratios in the present work is considered high, which may indicate the influence of the fossilization and diagenesis with the replacement of orthophosphate ion by carbonate ion in the apatite crystal lattice [37].

 doi:10.20944/preprints202603.0009.v1

The lowest CaO/P_2O_5 ratios suggest intense influence from terrigenous materials. The CaO/P_2O_5 ratio of the studied phosphate shows an average of 1.76, which may be due to either the substitution of PO_4 by CO_3 or the presence of calcite in the phosphorites [14]. The CaO/P_2O_5 ratio in phosphate rock typically ranges from 1.3 to 1.6, although it can reach up to 1.9 in certain deposits. This ratio is critical for processing; a lower ratio (e.g., 1.35) is preferred for reducing sulfuric acid consumption, while ratios above 1.6 indicate higher impurity levels. Pure fluorapatite has a ratio of approximately 1.32 [37].

The very strong correlation between Al_2O_3 vs. K_2O and TiO_2 indicates enrichment of these elements during the chemical weathering condition. On the other hand, the low positive relation between SO_3 and P_2O_5 (r =0.23) indicates that the sulfur may be formed by a diagenetic process, not by the action of bacteria in the formation of pyrite.

The trace and some rare earth elements in the present work are generally associated with detrital minerals due to weathering affecting, associated with organic matter, and those located within the apatite lattice, which is in agreement with [38]. Positive correlation between Sr and the other elements may reflect its stronger association with calcite than apatite. Ref. [39] Attributed Sr presence in phosphatic rocks to strontianite mineral. According to [40], increasing Zn content in phosphorites is linked to sulfate phases and substitution for Ca in apatite. The strong positive correlation of Zn with Fe and Ni is related to the partial substitution of Zn for calcium in the apatite lattice. The low Cu concentration reflects the absence of carbonaceous matter, which matches the results of [41], who reported Cu and Ni enrichment in organic-rich phosphorites. Low V content corresponds to its limited affinity for apatite.

Because of the low Th/U ratios, it is possible that different occurrences had different physicochemical circumstances during the secondary uptake of U. The concentration of uranium in the pore water and the length of exposure to that water are the primary factors influencing its accumulation. Additionally, the groundwater's Eh regulates the uranium exchange between phosphate particles and groundwater [42].

Meanwhile, the concentrations of the major oxides (P_2O_5, Fe_2O_3, and MgO) in the phosphatic rocks are used as an indicator for the industrial quality. Ref. [14] revealed that the phosphorites can be classified depending on the concentration of P_2O_5 content into: high grade (26–35% P_2O_5), medium grade (P_2O_5 ranging from 17-25%), and low grade (P_2O_5 from 12 to 16%). Therefore, the Wadi Hilal area is considered high-grade phosphorites with a P_2O_5 concentration of (28%) and medium-grade phosphorites with P_2O_5 concentrations (< 23%). The East Sibaiya area belongs to medium-grade phosphorites (P_2O_5 content of 26.54%) and low-grade phosphorites (P_2O_5 concentration of 19.46%). The Um Higarah area is related to high-grade phosphorites with P_2O_5 concentration (29.22%), and low-grade phosphorites with P_2O_5 concentration (< 23%). The Um Salama area has two phosphorite types: high-grade phosphorites with P_2O_5 concentration (31.24%) and low-grade phosphorites with P_2O_5 concentrations (< 23%). The Um Tundbah area has been classified into high-grade phosphorites with P_2O_5 concentration (29.79%) and low-grade phosphorites with P_2O_5 concentrations (< 23%).

5.4. Comparative Study

5.4.1. Average Major Oxides and Trace Elements

P_2O_5 ranges from 17.4% to 31.24% with an average of 23.72%. The value is higher than the averages of phosphate of the Red Sea region (16.43%, 23.65%, and 19.3%) recorded by [43–45], respectively (Figure 9; Table 4). Also, it is higher than the average values of the Nile Valley given by [43,44], but lower than the value in Abu Tartur that was mentioned by [44]; the Nile Valley of [45–49]. This value is also higher than the average values of the Abu Tartur phosphates of [43] Table 4; Figure 9.

Fluorine ranges from 0.65% to 1.49% (with an average of 1.3%), Table 4. This value is higher than the average of (0.95%) that was assumed by [46]. On the other hand, the average value of fluorine is

 doi:10.20944/preprints202603.0009.v1

lower than the average values (1.43%, 1.96%, and 2.99, respectively) reported by [47–49] Table 4; Figure 9.

Silica ranges from 7.76% to 27.81% (with an average value of 20.95%). This value is higher than the average values in the Red Sea (14.04% and 17.99%) of [43,44]. Besides, it's higher than the average values of [46–49] Table 4; Figure 9. Also, average silica is higher than the average value at Abu Tartur (14.66% and 11.54%, respectively). On the contrary, the average silica value is lower than the average values of the Nile Valley (26.90% and 37.01%) reported by [43,44], respectively.

Iron oxides represent a value that ranges of 1.16% to 1.90% (with an average of 1.49%). These value is higher than the average values in the Red Sea (0.23%, 1.05%, and 0.66%) that were introduced by [43,44,47], respectively. On the other hand, the average value of the studied phosphatic is lower than the Nile Valley (2.68% and 1.90%), and lower than the average values (4.17% and 4.73%) of Abu Tartur Table 4; Figure 9. Ref. [46,48,49] gives the average values (3.50%, 2.87%, and 2%, respectively) that are higher than the average value of the present work, Table 4; Figure 9.

Calcium oxide show value that ranges from 38.34% to 48.78% (with an average of 40.97%). These values are higher than the average values at the Nile Valley (28.67% and 31.86%, respectively) and at Abu Tartur (33.42% and 39.25%, respectively) that reported by [43,44]. Also, higher than the average values of the Red Sea (32.12%, 33.16, and 37.35%, respectively) of [43,45,48] Table 4; Figure 9. Meanwhile, it's comparable with the average values at the Red Sea (41.66%) that were summarized by [44]. On the contrary, it's lower than the average values at the Nile Valley (44.36%, 43.80%, 57.09%, and 44.60%, respectively) reported by [45–47,49] Table 4; Figure 9. Sulfur contents range from 0.25% to 1.44% (with an average of 0.65%), are comparable to the average value considered by [49], and lower than the average values (6.90%, 1.48%, and 1.12%, respectively) that were reported by [46–48].

Cr show value that ranges from 100.29ppm to 132.59ppm (with an average of 121.80%). These values are higher than the average values (113.25ppm) reported by [48]. Ni also ranges from 17.25 to 38.25 (with an average of 28.16ppm), Table 4. These value is higher than the average values (22ppm) of the Nile Valley reported by [45], and lower than the average values (469ppm, 77ppm, and 35.25ppm, respectively) at the Red Sea [45,47,48] Table 4.

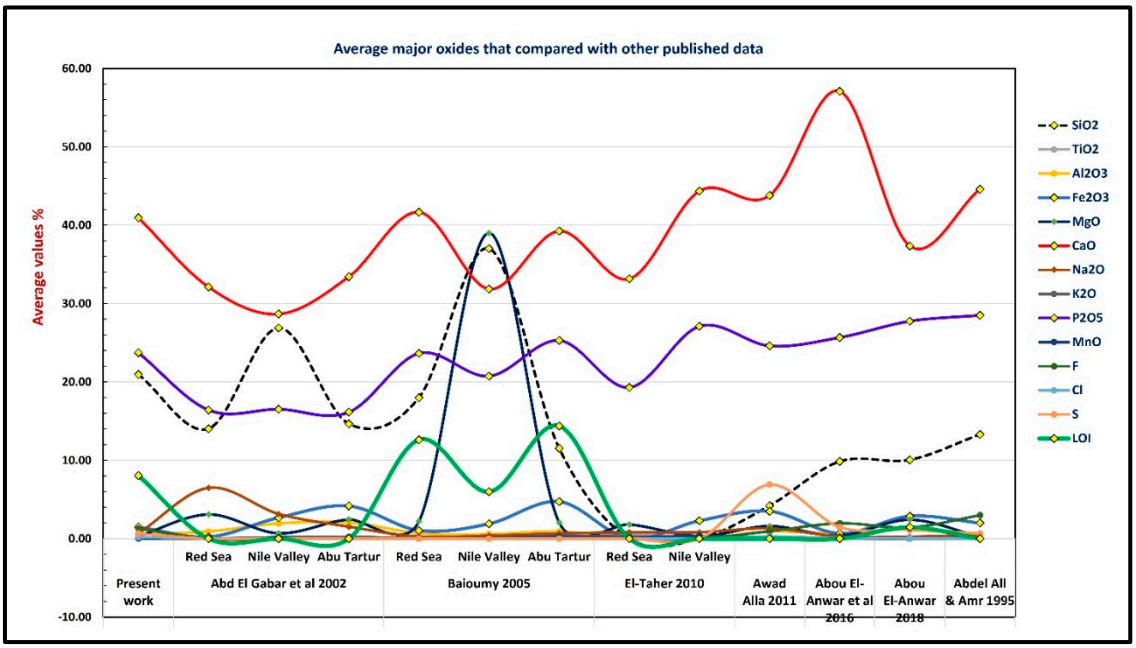

Figure 9. Average of major oxides in the present work compared with other published data in Egypt.

Cu represent value that ranges from 13.40ppm to 16.15ppm (with an average of 15.14ppm). These values are lower than the average values (18.25ppm) reported by [48]. Zn content in the present work ranges from 153.80 to 243.50 (with an average of 205.66ppm). These value is higher than the values of Red Sea, Nile Valley, and Abu Tartur (119.7ppm, 86.3ppm, 106.2ppm, respectively) [43],

 doi:10.20944/preprints202603.0009.v1

162ppm that is related to Nile Valley [45], and 133ppm, 149ppm, 68.25ppm, and 171ppm that were reported by [46–49]. On the other hand, the value is lower than (360ppm) at the Red Sea of [45]. Vanadium content ranges from 90.30ppm to 302.19ppm (with an average of 177.59ppm). V value is higher than the value (30ppm) of [46] and lower than the value at Nile Valley (220ppm) by [45] and 246ppm that was reported by [47] Table 4.

Table 4. Average major oxides and trace elements composition in the study area compared with other published average phosphates for different localities in Egypt.

Elements	Present work	Abd El Gabar et al 2002			Baioumy 2005			El-Taher 2010		Awadalla 2011	Abou El Anwar et al 2016	Abou El Anwar 2019	Abdel-All & Amer 1995
		Red Sea	Nile Valley	Abu Tartur	Red Sea	Nile Valley	Abu Tartur	Red Sea	Nile Valley				
SiO_2	20.95	14.04	26.90	14.66	17.99	37.01	11.54	ND	ND	4.20	9.85	10.06	13.30
TiO_2	0.02	0.01	0.09	0.05	0.03	0.04	0.05	0.67	ND	0.10	0.04	0.03	ND
Al_2O_3	0.53	0.92	1.94	2.06	0.70	0.58	0.91	ND	ND	0.90	0.70	1.24	0.62
Fe_2O_3	1.49	0.23	2.68	4.17	1.05	1.90	4.73	ND	2.29	3.50	0.66	2.87	2.00
MgO	0.33	3.09	0.68	2.45	2.19	39.00	2.05	1.82	0.33	1.60	0.37	2.41	0.23
CaO	40.97	32.12	28.67	33.42	41.66	31.86	39.25	33.16	44.36	43.80	57.09	37.35	44.60
Na_2O	0.66	6.48	3.15	1.52	0.26	0.39	0.66	0.81	0.81	1.30	0.26	0.24	0.50
K2O	0.03	0.02	0.20	0.24	0.08	0.09	0.40	0.29	0.10	0.20	0.05	0.03	0.15
P_2O_5	23.72	16.43	16.53	16.15	23.65	20.75	25.29	19.30	27.10	24.60	25.67	27.75	28.50
MnO	0.08	0.04	0.06	0.06	0.03	0.12	0.28	0.13	0.39	0.10	0.06	ND	ND
F	1.30	ND	ND	ND	ND	ND	ND	ND	ND	0.95	1.96	1.43	2.99
Cl	0.20	ND	ND	ND	ND	ND	ND	ND	ND	0.30	0.07	0.04	0.02
S	0.65	ND	ND	ND	ND	ND	ND	ND	ND	6.90	1.48	1.12	0.65
LOI	8.06	ND	ND	ND	12.62	5.98	14.38	ND	ND	ND	ND	1.46	ND
Cr	121.80	ND	ND	ND	ND	ND	ND	ND	ND	ND	ND	113.25	ND
Ni	28.16	ND	ND	ND	ND	ND	ND	469	22	ND	77	35.25	ND
Cu	15.14	ND	ND	ND	ND	ND	ND	ND	ND	ND	ND	18.25	ND
Zn	205.66	119.7	86.3	106.2	ND	ND	ND	360	162	133	149	68.25	171
Sr	1734.86	1385	1584	391	ND	ND	ND	520	1032	1001	1705	ND	1350
Zr	150.4	ND	ND	ND	ND	ND	ND	ND	ND	ND	ND	ND	ND
Ba	583.68	ND	ND	ND	ND	ND	ND	ND	ND	ND	ND	ND	ND
V	177.59	ND	ND	ND	ND	ND	ND	ND	220	30	246	ND	ND
Pb	5.62	ND	ND	ND	ND	ND	ND	ND	ND	ND	ND	ND	ND
CaO/P_2O_5	1.76	1.96	1.73	2.07	1.76	1.54	1.55	1.72	1.64	1.78	2.22	1.35	1.56

 doi:10.20944/preprints202603.0009.v1

5.4.2. Radioactive Elements

The average U values in the present work are 127.94 ppm (Table 5) that considered higher if compared with other published data, such as Gebel Hefhuf (western desert), followed by Wasief, Hammadat & Yonous (Red Sea), and Mahamied, Abu Had, West Nile Valley & SE Idfu (Nile Valley). Furthermore, the uranium concentrations through phosphorites of both the Nile Valley and Red Sea are close to each other (Table 5; Figure 10). The radioactive element concentrations in the present work, with data published previously, revealed that the U and Th values show a significant variety from one place to another (Figure 10).

Thorium value content is 1.57ppm (Table 5); these value considered low if compared with other published data [23,50]. The highest value of Th content belongs to Abu Tartur mine, Gebel Edmonstone, and Gebel Ghanima (Western Desert), followed by SE Idfu (Nile Valley), and Duwi, Hammadat, Yonous mine & Wasief at (Red Sea), Figure 10; Table 5. The least value of Th contents shows in Mahamied & Gebel Abu Had (Nile Valley), Wadi Araba & Gebel Sofraiyat (Sinai), followed by Gebel Sheikh Abdallah & Gebel Hefhuf (Western Desert), west Nile Valley (Nile Valley), Hammadat, Duwi, Wasief & Yonous mine (Red Sea) Figure 10; Table 5.

The low value of U content through the Western Desert is related to the fact that they lie high above the water table, under a very arid regime, and the absence of contact with basement rocks [22]. Ref. [21] Reported that these phosphorites formed under the shallowest depositional basins among all phosphorites of the economic belt in Egypt and received more accessory minerals and a higher content of the immobile elements (e.g., Th and REEs). In the Nile Valley region, the phosphorites of SE Idfu are related to the same phosphatic belt that also formed under a shallow basin and enriched in Th and REE [23].

The phosphorite at Gebel Hefhuf represent highest value of U content (100ppm; Table 5), approaching the maximum value recorded in the present work (127.94ppm), and is considered as exceptionally uraniferous with respect to those of the Western Desert. This may be related to the thermal gradient during the Oligo-Miocene age by basaltic intrusion that represents a direct contact with the phosphatic-bearing sediments [51]. The increasing of groundwater temperature leads to the increasing of uranium mobilization and trace elements. Under the control of the complicated structural framework (especially faults), many of the phosphorites in the Red Sea area have been in direct contact with groundwater for variable lapses of time. This may explain the high value of U in these phosphorites [23].

Thorium content ranges from 0.61 to 4.07ppm (with an average of 1.57ppm), Table 5. These value considered low compared with other published data. The average thorium content in the present work shows the least value, followed by the thorium content at the Wadi Araba and Gebel Sofraiyat (Sinai). Nile Valley and Red Sea, which have similar values, Figure 10; Table 5. The highest value of Th content belongs to Abu Tartur mine, followed by Gebel Ghanima, Gebel Edmonstone, Gebel Sheikh Abdallah, and Gebel Hefhuf (Western Desert), Figure 10; Table 5. The radioactive element concentrations in the present work, with data published previously, revealed that the U and Th values show a variety from one place to another Figure 10.

Th/U ratios displays a rather systematic distribution with highest values that range from 0.12 to 0.32 for phosphorites of the Gebel Ghanima, Abu Tartur, and Gebel Edmonstone (Western Desert), SE Idfu (Nile Valley), and Duwi mine (Red Sea), with low values (0.01 – 0.06) in the present work and for those of the other area (Table 5).

Table 5. Average radioactive element concentrations (ppm) in the studied phosphorite samples that compared with other published data in Egypt.

Area	Aver. Th	Aver. U	Th/U
Present work	1.57	127.94	0.01
Hammadat area	2.90	59.87	0.05
Duwi mine	3.50	22.77	0.15

 doi:10.20944/preprints202603.0009.v1

Wasief mine	2.30	66.70	0.03
Yonous mine	3.25	51.75	0.06
G Abu Had	1.83	49.00	0.04
Mahamied-Sibaiya	1.38	63.33	0.02
SE Idfu	4.74	24.75	0.19
West Nile Valley	2.29	46.07	0.05
G Ghanima	3.88	12.20	0.32
Abu Tartur mine	5.84	26.38	0.22
G Hefhuf	2.45	100.00	0.02
G Sheikh Abdallah	2.16	33.60	0.06
G Edmonstone	4.04	34.50	0.12
G Sofraiyat	1.78	33.78	0.05
Wadi Araba	1.41	26.86	0.05
MIN	1.38	12.20	0.01
MAX	5.84	127.94	0.32

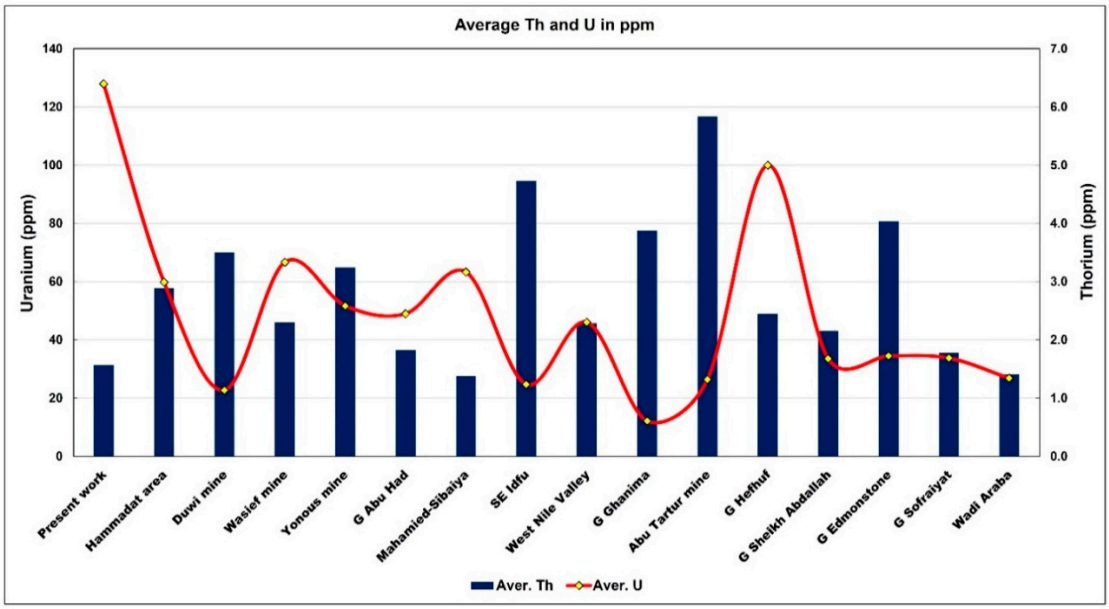

Figure 10. Average distribution of Uranium and Thorium in present work compared with various occurrences of the Egyptian phosphorites.

5.4.3. Rare Earth Elements

The average ∑REE, when compared with other published data, is illustrated in Table 6 and Figure 11. In the present work, the average of ∑HREEs (22.45 ppb) while the average of ∑LREEs (123.74 ppb). These value is higher than the values in Wadi Araba and Gebel Sofraiyat (Sinai), while ∑HREEs at Western Desert are 23.3 to 90.1, followed by West Nile Valley at the Nile Valley that gives ∑HREEs value 19.9, and at Hammadat & Duwi at the Red Sea that appears to have ∑HREEs content between 16.9 and 31.6. Also, the ∑HREEs have similar value with the Abu Had at the Nile Valley Table 6. On the contrary, ∑HREEs values are lower than the data of other work (e.g., Rabah mine at the Eastern Desert, Gebel Sheikh Abdallah, Abu Tartur & Gebel Hefhuf in the Western Desert, Mahamied & SE Idfu at the Nile Valley, and Wasief & Yonous at the Red Sea region Table 6; Figure 11.

On the other hand, the average ∑LREE contents in the study area 123.7ppb Table 6. In the Sinai Peninsula, the ∑LREE contents vary from 105.7ppb to 120.8ppb. These values are considered lower than the average value in the present work, Table 6, Figure 11. At Rabah mine, the ∑LREEs value is

 doi:10.20944/preprints202603.0009.v1

224.9ppb, and the Western Desert shows ∑LREEs contents from 159.6ppb to 656.1ppb. Also, the Nile Valley gives the ∑LREEs contents from 168.3ppb to 572ppb, while the ∑LREEs contents at the Red Sea range between 131.9ppb to 288.2ppb Table 6; Figure 11. These values are considered higher than the average value of the present work.

The highest values of the average of ∑REEs related to Gebel Sheikh Abdallah and Gebel Hefhuf (Western Desert) and SE Idfu (Nile Valley), Figure 11. Meanwhile, the moderate values of the average of ∑REEs within Egyptian phosphorites at the Wadi Araba and Gebel Sofraiyat (Sinai), Gebel Ghanima (Western Desert), Abu Had and Mahamied (Nile Valley), Hammadat, Yonous, and Wasief mine (Red Sea), Rabah mines (Eastern Desert), Figure 11; Table 6.

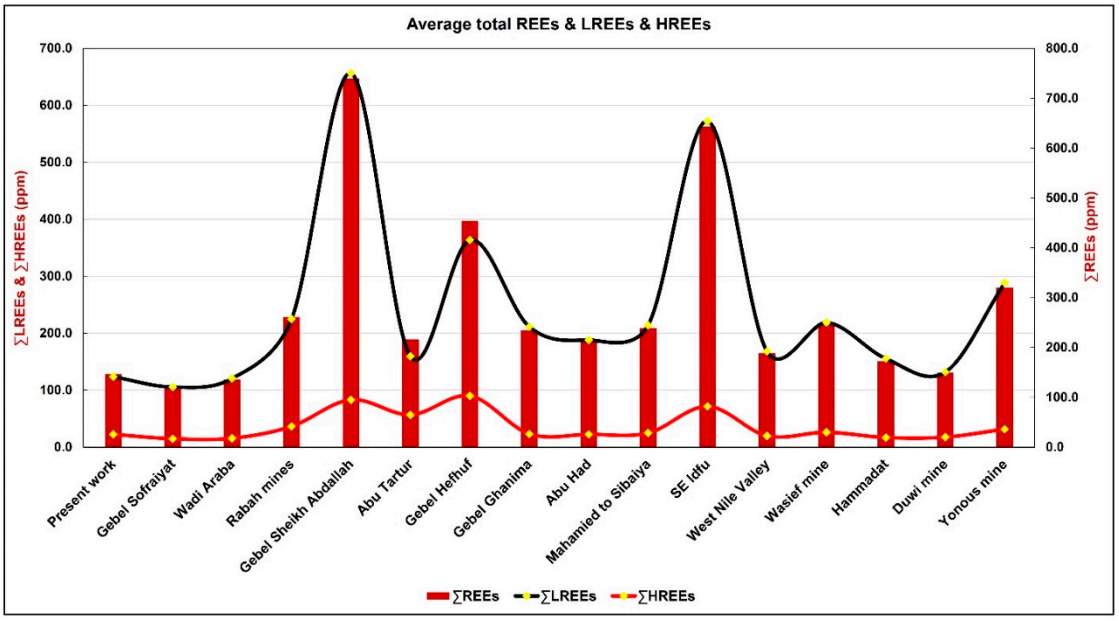

Figure 11. Average of the distribution of ∑REE, ∑LREE, and ∑HREE in the studied samples with various occurrences of phosphorites in Egypt.

Table 6. Average REEs (ppm) in the studied phosphorite samples that compared with other published data in Egypt.

Area	La	Ce	Pr	Nd	Sm	Eu	Gd	Tb	Dy	Ho	Er	Tm	Yb	Lu	∑LREEs	∑HREEs	∑REEs	Ce/La	Eu/Eu*
Present work	32.7	50.3	6.6	27.3	5.4	1.4	5.8	0.9	5.6	1.3	4.0	0.5	3.8	0.6	123.7	22.5	146.2	1.5	0.79
Gebel Sofraiyat	31.8	44.0	nd	22.9	5.5	1.4	5.6	0.9	5.5	nd	nd	nd	2.4	0.3	105.7	14.8	120.4	1.4	0.79
Wadi Araba	38.1	43.7	nd	32.2	5.3	1.5	5.6	0.9	5.1	nd	nd	nd	3.5	0.5	120.8	15.6	136.4	1.1	0.86
Rabah mines	60.5	86.5	nd	66.0	8.8	3.1	11.8	1.8	14.1	nd	nd	nd	7.5	1.3	224.9	36.5	261.4	1.4	0.91
Gebel Sheikh Abdallah	174.6	280.4	nd	156.9	34.3	10.0	31.0	4.9	28.9	nd	nd	nd	16.3	2.2	656.1	83.2	739.3	1.6	0.94
Abu Tartur	43.3	53.7	nd	46.4	10.0	6.2	8.2	1.7	8.7	nd	nd	nd	5.3	32.9	159.6	56.7	216.3	1.2	2.09
Gebel Hefhuf	79.6	129.0	nd	120.6	25.9	8.4	35.1	7.5	37.5	nd	nd	nd	8.9	1.1	363.5	90.1	453.6	1.6	0.85
Gebel Ghanima	55.0	91.8	nd	52.8	9.3	2.6	8.1	1.3	8.4	nd	nd	nd	4.8	0.7	211.6	23.3	234.8	1.7	0.92
Abu Had	43.2	80.2	nd	53.7	8.6	2.5	7.9	1.4	7.6	nd	nd	nd	4.9	0.8	188.1	22.5	210.5	1.9	0.93
Mahamied to Sibaiya	55.5	86.4	nd	60.4	9.4	2.4	8.5	1.5	8.7	nd	nd	nd	5.4	0.7	214.1	24.9	239.0	1.6	0.82
SE Idfu	155.3	239.5	nd	137.5	31.3	8.5	24.5	4.3	25.4	nd	nd	nd	14.9	2.4	572.0	71.5	643.5	1.5	0.94
West Nile Valley	49.9	68.9	nd	40.1	7.7	1.8	7.0	1.2	6.8	nd	nd	nd	4.3	0.6	168.3	19.9	188.2	1.4	0.77
Wasief mine	52.9	94.4	nd	59.6	9.2	2.7	8.9	1.4	9.6	nd	nd	nd	5.4	0.8	218.8	26.0	244.9	1.8	0.91
Hammadat	35.0	70.8	nd	40.5	7.4	1.9	6.0	1.2	6.0	nd	nd	nd	3.3	0.4	155.6	16.9	172.5	2.0	0.85
Duwi mine	30.0	59.7	nd	33.7	6.6	1.9	6.5	1.0	5.7	nd	nd	nd	3.9	0.6	131.9	17.6	149.4	2.0	0.90
Yonous mine	67.0	122.0	nd	80.3	15.0	4.0	11.9	1.9	10.0	nd	nd	nd	7.0	0.9	288.2	31.6	319.9	1.8	0.92

 doi:10.20944/preprints202603.0009.v1

Ce/La ratios in the study area are (1.4 – 1.6), in the Sinai area (1.1 – 1.4), the Eastern Desert provide Ce/La value of (1.4), while the Western Desert provides a range of (1.2 to 1.7). Meanwhile, the Nile Valley area gives a value of (1.4 to 1.9), while the Red Sea show value between 1.8 and 2 Table 6. Eu/Eu* ratios give values at the study area of 0.79, in the Sinai area, the ratios are 0.79 to 0.86, at the Eastern Desert, the Eu/Eu* ratio is 0.91, while in the Western Desert, the value ranging between 0.85 to 2.09, Nile Valley show values from 0.77 to 0.94, and the Red Sea region provide values range from 0.85 to 0.92 Table 6.

Positive Eu anomaly reveals an anoxic event before the phase of Late Cretaceous phosphate formation. Ce is a redox indicator. Mixing of seawater and upwelling during the Late Cretaceous was responsible for the recording of positive Eu and negative Ce anomalies in the Egyptian phosphorites [23].

The phosphorites in the Western Desert and Nile Valley, followed by the Red Sea region, are characterized by high concentrations of ∑REE compared with other regions. These higher ∑REE may be attributed to the higher abundance of pelletal apatite [52], and/or to the higher abundance of iron sulfide mineral (pyrite), which scavenges REE from seawater and associated sediments and transfers them diagenetically to the apatite. On the other hand, the weathered samples are slightly lower in LREE content. This may reveal the effective role of weathering in removing light REE [53]. The variations in REE content in the different types of phosphorites have been either attributed to changes in depositional conditions [54] or to mixing of chemical precipitates from seawater with land-derived detritus [55]. Weathering, burial diagenesis, and metamorphism may affect both REE concentrations and their distribution patterns in the phosphorites.

Ref. [39] Noted that REEs in phosphorites may be extracted as by-products during phosphoric acid production. LREEs enrichment relative to HREEs in the studied samples suggests post-depositional modification [56], which linked negative Ce and Eu anomalies in Egyptian phosphorites to formation under reducing conditions. The slight negative Ce and Eu anomalies observed here support a marine origin and a reducing depositional environment. Variability in REE content among phosphorite types has been attributed to differing depositional conditions [54].

The Ce/La ratio has little variation, revealing abnormal Ce enrichment due to extensive diagenetic alteration [57]. Positive Eu anomaly reveals an anoxic event before the phase of Late Cretaceous phosphate formation. Ce is a redox indicator. Mixing of seawater and upwelling during the Late Cretaceous was responsible for the recording of positive Eu and negative Ce anomalies in the Egyptian phosphorites. The average of REEs was normalized to the chondrite REE concentrations with reference values provided by [58] Figure 12. The patterns exhibit enrichment of LREEs relative to HREEs in the study area.

 doi:10.20944/preprints202603.0009.v1

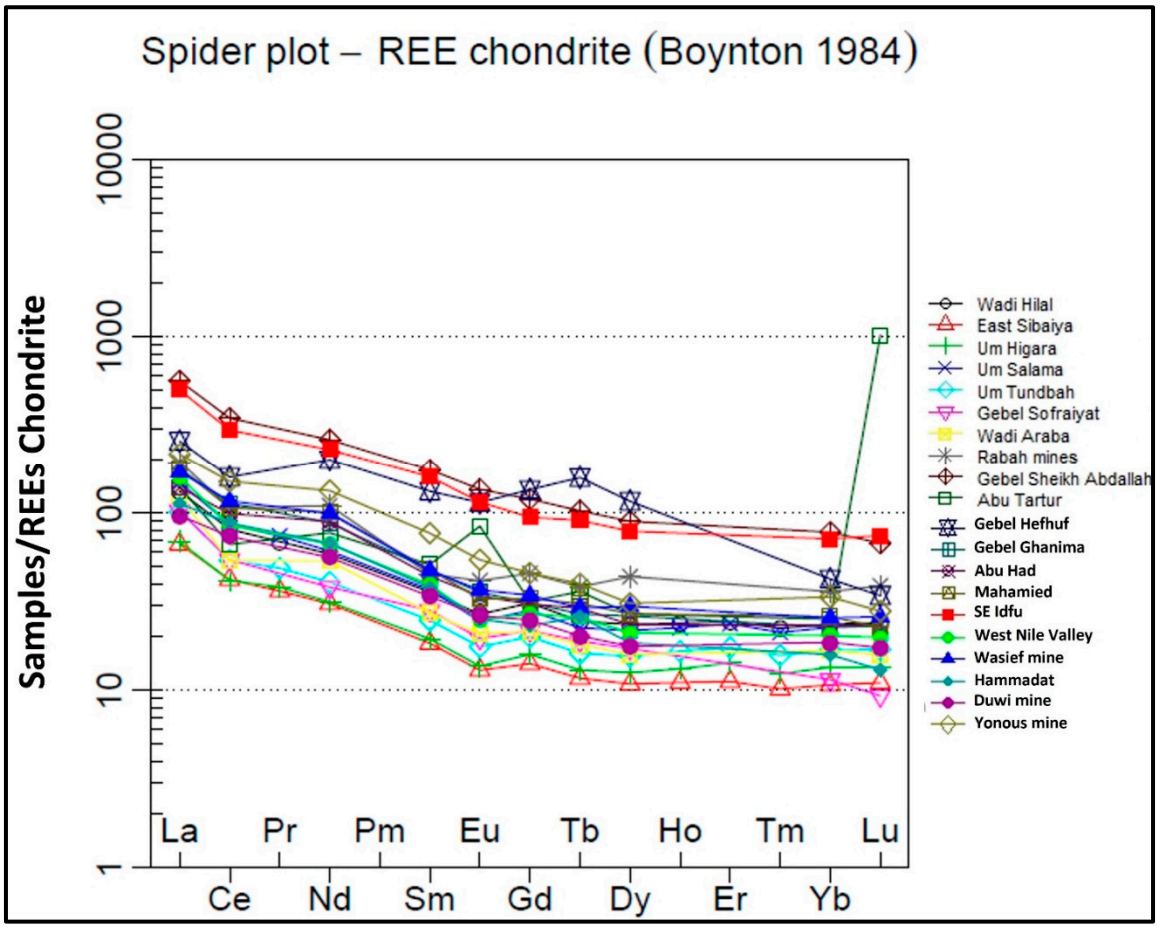

Figure 12. Chondrite normalized REE patterns of the average studied samples compared with various occurrences of phosphorites in Egypt.

6. Conclusions

Based on the obtained results from the current study, the following conclusions can be drawn:

- The stratigraphic and petrographic characteristics of the studied succession collectively reflect a progressive transition from continental siliciclastic settings to fully marine environments during the Late Cretaceous–early Paleocene.
- The Qusseir variegated shale marks the initial phase of this transition, recording low-energy coastal to delta-plain conditions influenced by alternating oxidation states and episodic clastic influxes. This unit represents the onset of marine encroachment over the Nubia Sandstone.
- The overlying Duwi Formation preserves the key stages of phosphorite formation on a shallow epicontinental shelf affected by Late Cretaceous global sea-level rise. Phosphogenesis was driven by high marine productivity, redox fluctuations, upwelling activity, and low sedimentation rates.
- The Dakhla shale records the maximum transgression and marks the shift from shallow-shelf phosphatic deposition to deeper, low-energy offshore sedimentation. Its fine-grained, organic-rich character indicates dysoxic bottom-water conditions conducive to enhanced preservation of organic matter.
- Petrographic evidence, such as abundant pellets, bioclasts, and reworked phosphatic grains, indicates oscillation between low and moderate energy conditions, allowing condensed phosphate accumulation. Associated lithofacies, including oyster limestone, marl, and chert, further confirm deposition under nutrient-rich, intermittently oxygen-deficient waters.
- Geochemical data support these interpretations. Silica is mostly detrital, with minor diagenetic microcrystalline forms. Variations in Fe_2O_3 reflect diagenetic oxidation of pyrite, whereas low

 doi:10.20944/preprints202603.0009.v1

MgO contents indicate minimal dolomitization. Trace-element relationships highlight the roles of lattice substitution and diagenetic redistribution, with Sr content linked to calcite and Zn enrichment related to its partial substitution for Ca in the apatite lattice.

- Light rare earth element patterns (LREE) enrichment and slight negative Ce and Eu anomalies indicate marine deposition under predominantly reducing conditions and subsequent post-depositional modification.
- The thermal activity related to the Oligo-Miocene age seems to be responsible for the high uranium and REEs contents.
- In general, the geological, petrographic, and geochemical evidence demonstrates that the Duwi phosphorites formed under conditions highly favorable for economically significant phosphate accumulation, shaped by upwelling-driven productivity, fluctuating redox conditions, and episodic sediment reworking across a shallow epicontinental shelf.

Author Contributions: Fatma S. Ramadan: supervision, investigation, and conceptualization. Abdel-Aal Abdel-Karim: supervision and conceptualization. Mokhles Azer: sample analysis. Hossam K. Sharaka: fieldwork, writing original draft, review, editing, drawing, and validation. Ahmed Khalil: writing original draft, fieldwork, and sample collections.

Funding: This research received no external funding. .

Data Availability Statement: The authors confirm that the data supporting the findings of this study are available within the article and its Supplementary Materials.

Conflicts of Interest: The authors declare no conflicts of interest.

Abbreviations

The following abbreviations are used in this manuscript:

REEs	Rare Earth Elements
HREEs	Heavy Rare Earth Elements
LREEs	Light Rare Earth Elements
XRF	X-Ray Fluorescence
ICP-MS	Inductively Coupled Plasma-Mass Spectrometry
LOI	Loss on Ignition

References

1. [1] Hermina, M.H., 1972, Review of the phosphate deposits of Egypt. Proceedings of the 2nd Arab Conference of Mineral Resources, Conf. papers, pp.109-149.
2. [2] Notholt, A.J.G., 1985, Phosphorite resources in the Mediterranean (Tethyan) phosphatic province: a progress report. Sciences G'eologiques, M'emoire 77, pp.9-17.
3. [3] Youssef, M. I., 1954, Stratigraphy of Gabel Oweina section near Esna, Upper Egypt, Bull. Inst. Desert Egypt, v. 4/ 2, pp. 83-93.
4. [4] Youssef, M.I., 1957, Upper Cretaceous rocks in the Qusseir area. Bull. Inst., Desert Egypt, 7, pp.35-54.
5. [5] Awad, G. H., and Ghobrial, M. G., 1966, Zonal stratigraphy of Kharga Oasis, Annals of the Geological Survey of Egypt, v.34, pp.1-77.
6. [6] El-Naggar, Z. R., 1966, Stratigraphy and planktonic foraminifer of the Upper Cretaceous-Lower-Tertiary succession in the Esna-Idfu region, Nile Valley, Egypt. Bulletin of the British Museum (Natural History), Geology Suppl., 2, 291p.
7. [7] El-Naggar, Z. R., 1970, The genus Rugoglobigerina in the Maastrichtian Sharawna shale, Egypt. Proceedings II Planktonic Conference, Roma, I, pp.477-537.
8. [8] Issawi, B., 1972, Review of Upper Cretaceous-Lower Tertiary stratigraphy in central and southern Egypt, Ann. Assoc. Petrol. Geol. Bull., 56/ 8, pp.1448-1463.

 doi:10.20944/preprints202603.0009.v1

9. [9] Issawi, B., Abdallah, A.M., and Said, M.M., 1978, Geology of Wadi El Mashash Area, Eastern Desert-Egypt. Ann. Geol. Surv. Egypt, 8, pp.163-185.
10. [10] Issawi, B., El-Hinnawi, M., Francis, M., and Mazhar, A., 1999, The Phanerozoic geology of Egypt: A geodynamic approach. Special Publication No. 76. Geol. Survey, Cairo.
11. [11] Klitzsch, E., and Wycisk, P., 1987, Geology of sedimentary basins of Northern Sudan and bordering areas. Ber. Gewiss. Abh, 75 (A), 1, pp. 97-136.
12. [12] Klitzsch, E., Groeschke, M., and Hermann-Degen, W., 1990, Wadi Qena: Paleozoic and Precambrian Cretaceous strata. In R. Said (ed.), The Geology of Egypt, Rotterdam, Balkema, pp. 321-327.
13. [13] Baioumy, H.M., Tada, R., 2005, Origin of Upper Cretaceous phosphorites in Egypt. Cretac. Res., 26, pp.261-275.
14. [14] Abou El-Anwar, E.A., Mekky, H.S., Abd El Rahim, S.H., Aita, S.K., 2017, Mineralogical, geochemical characteristics, and origin of Late Cretaceous phosphorite in Duwi Formation (Gebel Duwi Mine), Red Sea region, Egypt. Egyptian J Petrol, 26, pp.157–169.
15. [15] Abou El-Anwar, E.A., 2019a, Lithologic characterization of the phosphorite-bearing Duwi Formation (Campanian), South Esna, West Nile Valley, Egypt. Carbonates and Evaporates 34, pp.793-805.
16. [16] Abou El-Anwar, E.A., and Abd El Rahim, S.H., 2022, Mineralogy, geochemistry, and origin of the phosphorites at Um El-Huwtat mine, Qusseir, Central Eastern Desert, Egypt. Carbonates and Evaporites, 37:16, 18p.
17. [17] Youssef, M. I., 1949, Stratigraphical studies in Qusseir area. Ph. D. Thesis, Alex. Univ., Egypt, pp.35-54.
18. [18] Ghorab, M. A., 1956, A summary of proposed rock stratigraphic classification for the Upper Cretaceous rocks in Egypt. Geol. Soc. Egypt. April 9th.
19. [19] Said, R., 1962, The geology of Egypt. Elsevier, Amsterdam, 337p.
20. [20] El-Kammar, A., 1974, Comparative geochemical and mineralogical studies on Egyptian phosphorites. Ph.D. Dissertation, Geology Department, Faculty of Science, Cairo University, Giza, Egypt, 169p.
21. [21] Hassan, F., and El-Kammar, A.M., 1975, Environmental conditions affecting the accumulation of uranium and rare earths in Egyptian phosphorites. Egyptian Journal of Geology, v.19 (2), pp.169-178.
22. [22] Said, R., 1990, Geology of Egypt, A. A. Balkeina, Brockfield Rotterdam, Rotterdam, 722p.
23. [23] El-Kammar, A., and El-Kammar, M., 2002, on the trace elements composition of the Egyptian phosphorites: A new approach. 6th international conference on the geology of the Arab World, Cairo University, Feb., pp.227-244.
24. [24] El-Kammar, A.M., Darwish, M., Philip, G., and El-Kamaar, M.M., 1990, Composition and origin of black shales from Qusseir area, Red Sea. Egypt Journal of the University of Kuwait-Science, 17, pp.177-1989.
25. [25] Cook, P.J., and McElhinny, M.W., 1979, A reevaluation of the spatial and temporal distribution of sedimentary phosphate deposits in the light of plate tectonics. Economic Geology 74, pp.315 -330.
26. [26] Glenn, C.R., and Arthur, M.A., 1990, Anatomy and origin of a Cretaceous phosphorite-greensand giant, Egypt. Sedimentology, 37, pp.123–154.
27. [27] Lucas, J., Chaabani, F., and Prevot, L., 1979, Phosphorites et evaporates: deux formations de mileux sedimentaires voisins dans la coup Paleogene de Foum Selja (Metlaoui, Tunisie). Sci. Geol. Bull., v.32, pp.7-20.
28. [28] McHargue, T.R., and Price, B., 1982, Dolomite from clay in argillaceous or shale-associated marine carbonates. J Sed. Petro., v.52, pp.873-886.
29. [29] El-Kammar, A., and El-Kammar, M., 1996, potentially of chemical weathering under arid conditions of black shales from Egypt. J Arid Environments, v.33, pp.179-199.
30. [30] Tucker, M.E., 1984, Introduction to sedimentary petrology, Geoscience Texts, 3, London and Tonbridge, 252p.
31. [31] Cathcart, J., and Gulbradsen, R., 1973, Phosphate deposits, U.S. Geol. Surv., Prof. Paper, pp.820-515.
32. [32] Zidan, I.H., 2014, Evaluation of phosphorite and Uranium in Lower phosphorite Member, Duwi Formation at Kummer area, South Esna, West Nile Valley, Egypt. Sedimentology of Egypt, 21, pp.143-154.

 doi:10.20944/preprints202603.0009.v1

33. [33] De Silva, E.F.D., Ammar, M., Celso, G., Fernando, N., Abdelkrim, C., Cristina, S., Valdemar, E., Ana, R., and Marques, F., 2010, Heavy elements in the phosphorite from Kalaat Khasba mine (North-western Tunisia): potential implications on the environment and human health. J Hazard Mater., 182, pp.232–245.
34. [34] McConnell, D., 1973, Apatite, its crystal chemistry, mineralogy, utilization, and geologic and biologic occurrences, New York.
35. [35] Blatt, D., Middleton, G., and Murray, R., 1972, Origin of sedimentary rocks. Prentice-Hall, New Jersey.
36. [36] Dabous, A. A., 1981, Mineralogy, geochemistry, and radioactivity of some Egyptian phosphate deposits. Ph.D. Thesis. Florida State Univ. College of Arts and Sciences. 201p.
37. [37] Nemliher, J. G., Baturin, G. N., Kallaste, T. E., and Murdmaa, I. O., 2004, Transformation of hydroxyapatite of bone phosphate from the ocean bottom during fossilization. Lithology Mineral Resources. 39, pp.468-479.
38. [38] El-Kammar, A.M., Zayed, M.A., Amer, S.A., 1979, Rare earths of the Nile Valley phosphorites, Upper Egypt. Chem Geol., 24, pp.69-81.
39. [39] Zidan, I.H., 2002, Geological and Geochemical studies of Abu-Tartur phosphate, Western Desert, Egypt, Ph. Fac. Sci., Al-Azhar Univ., 235p.
40. [40] Altschuler, Z.S., 1980, The geochemistry of trace elements in marine phosphorites, part I: characteristic abundances and enrichment. In: Bentor YK (ed) Marine phosphorites, Spec Publication. 29, pp.19-30.
41. [41] Basta, E., and El Kammar, A. M., 1976, Mineralogy and geochemistry of the phosphorites of Abu Tartur, WesternDesert, Egypt. The 25th International Geological Congress, Sydney, Australia, 2, Section 14, 555p.
42. [42] Weinberg, J.M., and Cowart, J.B., 2001, Hydrogeologic implications of uranium-rich phosphate in northeastern Lee County. In: Missimer, T.M. and Thomas, M.S. (Eds.), Geology and Hydrogeology of Lee County, Florida. Florida Geological Survey Special Publication No. 49, pp.151-165.
43. [43] Abd El-Gabar, M., El-Arabia, I., and Khalifa, H., 2002, Application of multivariate statistical analyses in the interpretation of geochemical behavior of uranium in phosphatic rocks in the Red Sea, Nile Valley and Western Desert, Egypt. J. Environ. Radioact., 6, pp.169-190.
44. [44] Baioumy, H.M., 2005, Preliminary data on cadmium and arsenic geochemistry for some phosphorites in Egypt. Journal of African Earth Sciences, 41, pp.266-274.
45. [45] El-Taher, A., 2010, Elemental analysis of two Egyptian phosphate rock mines by instrumental neutron activation analysis and atomic absorption spectrometry. App Radiat Isot., 68, pp.511-515.
46. [46] Awadalla, G.S., 2011, Geochemistry and microprobe investigations of Abu Tartur REE-bearing phosphorite, Western Desert, Egypt. Journal of African Earth Sciences, 57, pp.431-443.
47. [47] Abou El-Anwar, E.A., Mekky, H.S., Abd El Rahim, S.H., Aita, S.K., 2017, Mineralogical, geochemical characteristics, and origin of Late Cretaceous phosphorite in Duwi Formation (Geble Duwi Mine), Red Sea Region, Egypt. Egyptian J Pet., 26, pp.157–169.
48. [48] Abou El-Anwar, E.A., 2019, Lithologic characterization of the phosphorite-bearing Duwi Formation (Campanian), South Esna, West Nile Valley, Egypt. Carbonates and Evaporites, 34, pp.793–805.
49. [49] Abdel-All, E.A., and Amer, A.M., 1995, Evaluation of Sibaiya-West phosphate concentrate for nitrophosphate fertilizer production. Miner. Eng., 8(10), pp.1221–1230.
50. [50] Ismael, I.S., 2002, Rare Earth Elements in Egyptian Phosphorites. Chinese Journal of Geochemistry, v. 21 (1), 10p.
51. [51] Meneisy, M.Y., and Kreuzer, H., 1974, Potassium-Argon ages of Egyptian basaltic rocks. Geol. Jb., D9, pp.21-31.
52. [52] Germann, K., Bock, W.D., and Schroter, T., 1984, Facies development of Upper Cretaceous phosphorites in Egypt: sedimentological and geochemical aspects. Berliner Geowiss. Abh., 50, pp.345-361.
53. [53] McArthur, J.M., and Walsh, J.N., 1984, Rare-earth element geochemistry of phosphorites. Chem. Geol., 47, pp.191-220.
54. [54] Altschuler, Z.S., Berman, S., Cuttita, F., 1967, Rare earths in phosphorites: Geochemistry and potential recovery. U.S. Geological Survey Professional Papers 525b, pp.1-9.
55. [55] Kolodny, Y., 1981, Phosphorites. In: Emiliani, C. (Ed.), The Sea, J. Wiley & Sons, New York, 7, pp. 981-1023.

 doi:10.20944/preprints202603.0009.v1

56. [56] Baioumy, H.M., 2011, Rare earth elements and sulfur and strontium isotopes of upper Cretaceous phosphorites in Egypt. Cretaceous Research, v. 32(3), pp.368-377.
57. [57] Mazumdar, A., Banerjee, D., Schidlowski, M., and Balaram, V., 1999, Rare earth elements and stable isotope geochemistry of Early Cambrian chert-phosphorite assemblages from the Lower Tal Formation of the Krol Belt, Lesser Himalaya, India. Chem. Geol., 156, pp. 275-297.
58. [58] Boynton, W.V., 1984, Geochemistry of the REE: meteorite studies. In: Henderson, P. (Ed.), Rare Earth Element Geochemistry. Elsevier, pp.63–114.
59. [59] Egyptian Geological Survey and Mining Authority, 1968, Geological map of Idfu-Qena area, scale 1:200.000, phosphate project group between Soviet and EGSMA, unpublished – internal report.